SEMARAK ILMU
PUBLISHING

Journal of Advanced Research in Fluid
Mechanics and Thermal Sciences

Journal homepage:
https://semarakilmu.com.my/journals/index.php/fluid_mechanics_thermal_sciences/index
ISSN: 2289-7879

Analysis of Base Pressure Control with Ribs at Mach 1.2 using CFD Method

Ahmad ‘Afy Ahmad Fakhruddin[1], Fharukh Ahmed Ghasi Mahboobali[2], Ambareen Khan[3], Mohammad Nishat Akhtar[3], Sher Afghan Khan[1,*], Khizar Ahmed Pathan[4]

[1] Department of Mechanical & Aerospace Engineering, Faculty of Engineering, IIUM, Gombak Campus, Kuala Lumpur, Malaysia
[2] Government Engineering College Gangavathi Koppal, District Karnataka - 583 227, India
[3] Department of Aerospace Engineering, School of Engineering, USM, Penang, Malaysia
[4] Department of Mechanical Engineering, Chh. Shahu College of Engineering, Aurangabad, 431011, India

ARTICLE INFO

Article history:
Received 16 June 2024
Received in revised form 5 October 2024
Accepted 15 October 2024
Available online 30 October 2024

ABSTRACT

This paper discusses the control of base pressure by passive means, where the jet is issued from a converging nozzle at sonic Mach number under a favorable pressure gradient. The effect of employing annular ribs on the enlarged duct and its impact on the flow field, as the passive control mechanism from a converging nozzle at the sonic Mach number, is investigated numerically in this study. The velocity distribution and base pressure changes are analyzed using a numerical compressible turbulence flow model. Initially, the rib is positioned at 16 mm (1D) from the base of the duct. Later, the rib position is shifted from 1D to 2D and then to 3D and 4D. The effect of variation of the rib positions, as well as its height from 1 mm to 3 mm, keeping the width of the rib fixed to 3 mm, is studied. The nozzle pressure ratio varies from 1.5 to 5, and the rib location is 1D and 2D. The velocity variation in the duct with and without rib placement is also analyzed. The results revealed comprehensive spread observations from the positive analysis of base pressure variation in ducts with no ribs and ribs with heights of 1 mm and 2 mm. The base pressure increased significantly with increasing nozzle pressure ratio for both rib heights compared to a smooth duct. It is also deduced that the highest base pressure is achieved at an aspect ratio of 3:1 when placed at 4D.

Keywords:
Supersonic; base pressure; Mach; ribs; passive control

1. Introduction

The compressible flow effects dominate high-speed aircraft, rockets, reentry vehicles, projectiles, external ballistics, etc. During the subsonic and supersonic flow regimes, the flow is compressible, and the density of the air varies. These variations in density need to be considered when designing high-speed vehicles. At a very high Mach number, aerodynamic heating becomes a severe problem that must be addressed. The aerodynamics at high Mach numbers is different from the supersonic flow. The linearized theory cannot be used at transonic Mach numbers.

---

[*] *Corresponding author.*
E-mail address: sakhan@iium.edu.my

https://doi.org/10.37934/arfmts.123.1.108143

During the evolution of the linearized theory, the second-order terms were neglected as their order of magnitude was very small compared to the first-order terms. However, this assumption fails when the Mach number is closer to unity. The transonic flow is studied through the internal flow method in the present study. Here, the flow from a converging nozzle is suddenly exhausted into a circular duct of larger diameter. Due to the sudden expansion, the flow is separated while exiting from the nozzle and forming the wake region at the base. The jet pump action in these flows leads to base corner flows where the base pressure is low, as shown in Figure 1.

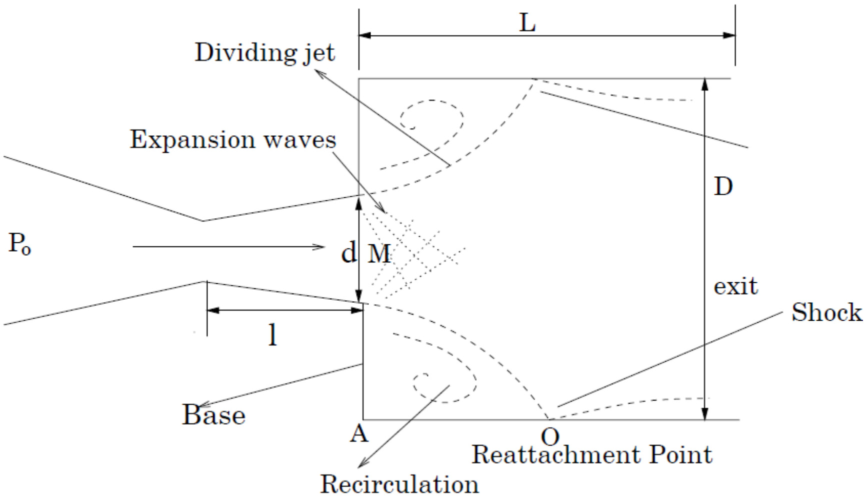

Fig. 1. A view of the sudden expansion flow from the converging nozzle

The low pressure at the corner causes the base drag flows, and this may account for up to 60 % of the total drag, which must be considered at the design stage and needs urgent attention to augment its magnitude and, hence, the optimization of the aerodynamic shape of the aerospace vehicles. Active and passive control methods are often adopted to increase base pressure [1-4]. Khan and Rathakrishnan [5] did experimental studies to control the base pressure from over-expanded nozzles for Mach numbers ranging from 2 to 3. Results show that at these Mach numbers, the microjet control decreases the pressure for all the Mach numbers and area ratio as the jets are over-expanded for all the Mach numbers except for Mach 2. With the increase in the Mach number as well as the area ratio, the reattachment length will increase, and the same results were observed by Khan and Radhakrishnan [5] when they conducted the experiments for an under-expanded case for Mach numbers 1.25, 1.3, 1.48, 1.6, 1.8, 2.0.

The experimental studies using internal flow test setup have many distinct advantages compared to exterior ballistics tests conducted in the ballistics range for Shells, unguided rockets, bombs, and missiles. An adequate air supply is necessary for tunnels with the test sections so that the wall interference does not disturb the flow over the model. Support mechanisms like stings used to support the model are eliminated, which is vital for external flow while performing the internal flow experimental analysis. The internal flow setup has the added advantage of static pressure, and the whole temperature of surface body measurement can be performed in the corner of the wake region and at the inlet section of the expansion portion. The tests conducted in such a way are significant as they provide theoretical predictions accurately [5-15].

Korst [16] studied the problem of base pressure in transonic and supersonic flow, where the incoming flow at the base was sonic and supersonic after the wake. Depending upon the interaction among the adjacent free stream and the dissipative shear flow considering the mass in the wake, Korst devised a model based on the physics of the transonic and supersonic flow. Anderson and Williams [17] studied the sudden expansion of air by analyzing the noise produced and the resulting base pressure in a cylindrical duct. The base pressure obtained was minimal due to the attached flow depending upon the duct-to-area ratio of the nozzle. Their results reveal that whenever the base pressure is minimum, that corresponds to the minimum noise the jet produces.

Khan and Rathakrishnan [18] used microjets as a control mechanism to control the base pressure for Mach number numbers in the range from 1.25 to 3. Their results show that microjets can lower Mach numbers and area ratios, and the resulting base pressure assumes very high values. The physics behind this trend is mainly due to the jet becoming under-expanded at these Mach numbers. It is well known that the control, either active or passive, becomes effective under a favorable pressure gradient. In their test, the NPRs considered were such that up to Mach 2, the jets were under, over, and correctly expanded. However, for Mach (M), more than two of the NPRs tested were over-expanded. The expansion level may be why the control in the form of microjets was effective at higher Mach numbers and area ratios.

Vikramaditya *et al.,* [19] investigated the pressure-flow variations experimentally in the base region of a characteristic missile shape at a free stream subsonic flow of Mach number 0.7. Their purpose was to characterize the base pressure-flow variations and explain the effect of base cavities on their performance. They conducted experiments for unsteady pressure measurements at six azimuthal positions. Significant fluctuations in pressure-flow characteristics were observed laterally in the azimuthal direction due to the irregularity of the model. The base cavities were realized to improve the base pressure and decrease the root mean square of the pressure variations. They showed that the higher-order moments provide a lessening tendency as the length of the base cavity is augmented.

Jaimon *et al.,* [20] used the L9 orthogonal array to plan experiments and found that the lower area ratios are more useful in control than the higher area ratios. Analysis of variance and multiple linear regression analysis were performed to obtain experimental results. Fifteen random test results were used to predict accuracy and test two linear regression models. Their study revealed that the linear regression model is enough to predict the base pressure accurately with and without control. Computational fluid dynamics analysis was performed for further in-depth analysis, and validation of the experimental results was presented.

The flow field became oscillatory for a particular NPR and L/D ratio combination. The oscillatory nature of the flow in the duct was observed in both control and without-control cases. Other relevant research works using active control include [20-27]. Pathan *et al.,* [25] delved into how the level of expansion affects base pressure and reattachment length. Their results confirmed that conditions significantly impact pressure and flow behavior. This further emphasizes the need to consider dynamics when developing strategies for optimizing base pressure.

Mechanisms for Controlling Base Pressure Base pressure plays a role in understanding how objects behave in high-speed airflow. Researchers have explored methods to regulate and improve base pressure. These methods include techniques like incorporating ribs and using jet flow management. The studies by Shaikh *et al.,* [28,29] focused on converters and analyzed flow and pressure drop uniformity within the monolith. This research offers valuable insights into managing pressure fluctuations in intricate flow systems. While not directly linked to base pressure, their findings underscore the significance of optimizing flow properties for better pressure regulation.

Various studies have used Computational Fluid Dynamics (CFD) to study and improve how fluids move in duct systems and high-speed settings [30-40]. For instance, Pathan *et al.,* [30] looked into optimizing the length of ducts for flows that suddenly expand. Their findings shed light on how changes in shape can influence pressure. Similarly, they examined factors impacting thrust and base pressure inflows, revealing that the design of the nozzle and the level of expansion play roles in pressure [31]. Khan *et al.,* [37] conducted a CFD study on submarines to reduce resistance. This indirectly aids in grasping pressure management through streamlining around submerged objects. The findings showcase the real-world utility of CFD and endorse using simulation results for experimental verification. The arrangement of ribs in a duct system can impact base pressure. Aqilah *et al.,* [38] explored the use of control to influence flow at speeds by varying the placement of ribs. Their detailed study showed how rib positioning affects base pressure [38]. This research supports the idea that passive control techniques, like rib placement, can effectively alter flow patterns and improve base pressure. The characteristics of flow, including levels of expansion and pressure ratios, are crucial for controlling base pressure. In a study by Fiqri *et al.,* [39], the impact of flow on pressure was examined at sonic Mach numbers. Their findings demonstrated how the configurations of expansion and cavities influenced base pressure. This research underscores the relationship between flow characteristics and pressure dynamics, which is vital for creating effective control systems.

Other studies by Shamitha *et al.,* [41,42] focused on how pressure is distributed on speed wedges. This research provided insights into how pressure varies under conditions and different flow scenarios. Understanding these dynamics, including base pressure control, is crucial for pressure distribution management. Similarly, Shaikh *et al.* investigated how the angle of a cone impacts pressure distribution on its surface. That indirectly relates to the design and positioning of passive control features such as ribs. Their findings highlight factors' significance in effectively managing pressure [43-45].

The control of pressure at the corner of the duct, when the flow exits from the nozzle is achieved using several methods. Priority is given to the flow regime analysis for different Mach numbers and duct designs, and significant contributions are made through experimental techniques. However, the reviewers do not conduct in-depth fluid flow simulation analysis using any numerical method. This work uses a turbulent numerical model to investigate the effect of the rib locations and their height when the duct diameter is 16 mm, i.e., the area ratio is fixed at 2.56. Base pressure regulation with an annular rib creates a disturbance in the field. Hence, a new flow field is analyzed using the velocity distribution and streamline contours. When the NPR is increased, the flow expands with a certain level of under-expansion and correct expansion, which has a different flow phenomenon. The present study is undertaken to understand the behaviors of the flow field in the suddenly expanded duct and the physics behind these phenomena.

2. Problem Definition

There are numerous critical issues impacting base flows. A few vital parameters are Mach number, boundary layer type before the separation, and geometry. Numerous studies have explored the influence of passive control devices, such as ribs. However, a comprehensive understanding of how rib geometry affects suddenly expanded flows remains elusive. This research aimed to address the knowledge gap by conducting experimental investigations focused on the specific context of flow characteristics through suddenly expanded ducts at Mach 1.2. By utilizing the power of passive control strategies, we can optimize the aerodynamic performance of high-speed vehicles operating at Mach 1.2, making them more efficient, stable, and capable of achieving their mission objectives. Continued advancements in this area hold the potential to revolutionize the design and operation of supersonic vehicles, pushing the boundaries of speed, efficiency, and safety in aerospace engineering.

The Computational Fluid Dynamics (CFD) software used throughout the procedure was ANSYS Workbench, which used Fluid Flow (Fluent) analytical methods. The model was created using a Design Modeller. Figure 2 illustrates a converging nozzle that suddenly expands into a duct with five ribs. Referring to Radhakrishnan's [46] experimental setup, the dimensions for the convergent-divergent nozzle with suddenly extended circular are shown in Table 1. The duct length, L, varies according to the L/D ratio, which ranges from one to six.

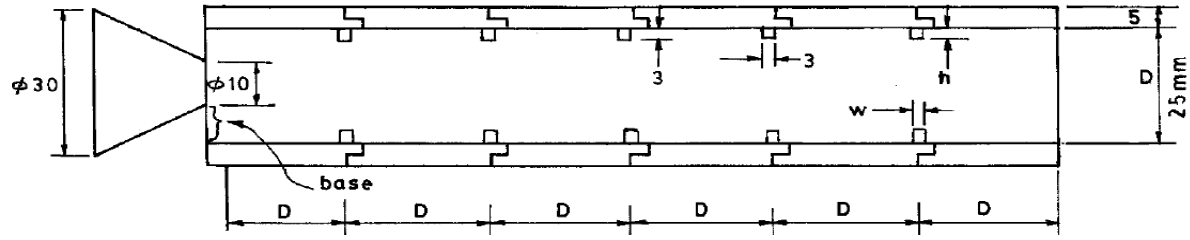

Fig. 2. A duct with five ribs used in the experimental study [28]

Table 1
The geometries of the validation model

Nozzle Dimension	Values
Nozzle inlet diameter	30 mm
Nozzle outlet diameter	10 mm
Duct diameter	22 mm
Duct length	Varies from 1D to 6D
Converging length	20 mm
Rib width	3 mm
Rib height	Varies from 1mm to 3mm

3. Computational Fluid Dynamics

The CFD process comprises several vital steps that facilitate experimentation and analysis. It begins with modeling, which defines the system's geometry and governing equations. Subsequently, meshing is performed to discretize the domain for numerical calculations. Pre-processing involves setting up simulation parameters and boundary conditions, ensuring an accurate representation of the real-world system. The solution phase employs computational methods to solve fluid equations and simulate fluid flow within the nozzle. Finally, post-processing analyzes and visualizes the simulation results, providing valuable insights that guide experimentation and design decisions. CFD is widely used for a variety of reasons, including its low cost when compared to physical experiments and tests for obtaining essential engineering data for design, its high-speed calculation process, which allows simulations to be completed in a short period, and its ability to simulate real and ideal conditions over physical processes.

3.1 Governing Equations

The flow through the nozzle is considered turbulent; hence, the k-standard model is applied for the compressible flow field. The flowing equations most appropriately represent the turbulent flow field.

Continuity equation for the compressible flow (density ρ based) with the steady-state condition in the 2-dimensional cylindrical coordinate system

$$\frac{1}{\mathrm{r}}\frac{\partial(\rho\mathrm{ru})}{\partial\mathrm{r}}+\frac{\partial(\rho\mathrm{v})}{\partial\mathrm{z}}=0 \tag{1}$$

The time-averaged axial z-momentum equation representing u velocity of flow is given by

$$\frac{1}{r}\frac{\partial(\rho r u u)}{\partial z}+\frac{1}{r}\frac{\partial(\rho v u)}{\partial r}=-\frac{\partial p}{\partial r}+(\mu+\mu_t)\frac{\partial}{\partial z}\left[2\frac{\partial u}{\partial z}-\frac{2}{3}(\nabla.\vec{v})\right]+(\mu+\mu_t)\frac{\partial}{\partial r}\left[\frac{\partial u}{\partial r}+\frac{\partial v}{\partial z}\right] \quad (2)$$

The radial r-momentum equation for v velocity

$$\frac{1}{r}\frac{\partial(\rho r u v)}{\partial z}+\frac{1}{r}\frac{\partial(\rho v v)}{\partial r}=-\frac{\partial p}{\partial r}+(\mu+\mu_t)\frac{\partial}{\partial r}\left[\left(2\frac{\partial u}{\partial z}-\frac{2}{3}(\nabla.\vec{v})\right)\right]+(\mu+\mu_t)\frac{\partial}{\partial z}\left[\left(\frac{\partial u}{\partial r}+\frac{\partial v}{\partial z}\right)\right]-2\frac{(\mu+\mu_t)v}{r^2}+\frac{2}{3}\frac{1}{r}(\mu+\mu_t)(\nabla.\vec{v}) \quad (3)$$

The term $\vec{v}$ in Eq. (2) and Eq. (3) is given by

$$\nabla.\vec{v}=\frac{\partial u}{\partial z}+\frac{\partial v}{\partial r}+\frac{v}{r} \quad (4)$$

Here, μ is viscosity, μo is the reference viscosity value in kg/m-s, T is static temperature, and To is the reference temperature in K. S is Sutherland constant depending upon effective temperature. The quantity $\left(\frac{k}{C_p}+\frac{\mu_t}{Pr_t}\right)$ represents the valuable thermo-physical property of fluid where k is the thermal conductivity in W/m2k, Cp is the specific heat capacity in KJ/kg-K, μ_t is turbulent viscosity in kg/m-s, and Pr_t is the Prandtl number for turbulent flow.

The K-ε turbulence model is among the famous models providing economy, robustness, and sufficient accuracy for many flow situations. The k-ε turbulence model employed in this work is made available by the Ansys Fluent software. The turbulent kinetic energy, i.e., K-equation, is given by

$$\frac{\partial(\rho u K)}{\partial z}+\frac{1}{r}\frac{\partial(\rho v K)}{\partial r}=\frac{\partial}{\partial z}\left[\left(\mu+\frac{\mu_t}{\sigma_k}\right)\frac{\partial K}{\partial z}\right]+\frac{1}{r}\frac{\partial}{\partial r}\left[r\left(\mu+\frac{\mu_t}{\sigma_k}\right)\frac{\partial K}{\partial r}\right]-\rho\varepsilon+G \quad (5)$$

The term σ_k is the turbulent Prandtl number for K, ε is the turbulent kinetic energy dissipation rate, and G is the turbulence generation term given by

$$G=\mu_t\left(\frac{\partial u_i}{\partial x_j}+\frac{\partial u_j}{\partial x_i}\right)\frac{\partial u_i}{\partial x_j}-\frac{2}{3}k\delta_{ij}\frac{\partial u_i}{\partial x_j} \quad (6)$$

The kinetic energy of turbulence dissipation, i.e., ε-equation, is given by

$$\frac{\partial(\rho u \varepsilon)}{\partial z}+\frac{1}{r}\frac{\partial(\rho v \varepsilon)}{\partial r}=\frac{\partial}{\partial z}\left[\left(\mu+\frac{\mu_t}{\sigma_\varepsilon}\right)\frac{\partial \varepsilon}{\partial z}\right]+\frac{1}{r}\frac{\partial}{\partial r}\left[r\left(\mu+\frac{\mu_t}{\sigma_\varepsilon}\right)\frac{\partial \varepsilon}{\partial r}\right]-C_1 f_1\left(\frac{\varepsilon}{K}\right)G-C_2 f_2\left(\frac{\varepsilon^2}{K}\right) \quad (7)$$

The term $\mu_t=\rho f_\mu C_\mu k^2/\varepsilon$ represents turbulent viscosity, the value of C_μ, C_1, C_2, f_μ, σ_k, σ_ε are all arbitrary constants.

3.2 Geometry and Modelling

In this study, the geometry model without passive control, which is a converging-diverging nozzle with a plain duct, will be used to assess the efficiency of passive control and flow development in detail due to the existence of ribs. Then, passive control (ribs) is applied to the duct to manipulate its flow development. The rib form is rectangular, as illustrated in Figure 3.

Fig. 3. The rectangular-shaped rib

The width of the ribs is kept constant, which is 3mm, but the ribs' height varies. The rib's dimensions are shown in Table 2 below.

Table 2
The rib's dimensions

Width (mm)	3	3	3
Height (mm)	1	2	3

In this work, the ribs' locations from the base pressure wall varied to 0.5D, 1D, 1.5D, 2D, 3D, and 4D, as shown in Table 3. The ribs' locations were calculated using the equations below

$$Ribs\ Location, RL = D - \frac{w}{2}; D = 16\ mm,\ w = 3mm$$

Table 3
Ribs location and its distance from the base wall

Location	0.5D	1D	1.5D	2D	3D	4D
Distance from the base wall	6.5 mm	14.5 mm	22.5 mm	30.5 mm	46.5 mm	62.5mm

Figure 4 illustrates an experimental setup featuring a convergent-divergent axisymmetric nozzle that suddenly expands into a larger cross-sectional area within a circular duct with an annular rib. The present work dimensions and parameters manipulated in this project are shown in Table 4 below.

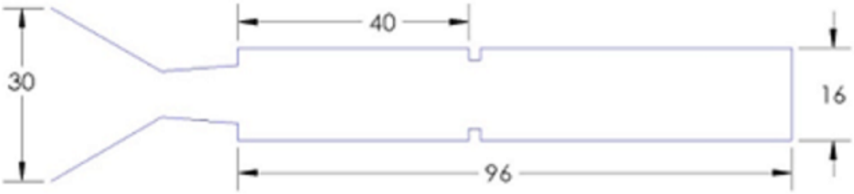

Fig. 4. Schematic diagram of the nozzle with the enlarged duct

Table 4
Present work dimensions and parameters

Parameters	Original Value
Mach number	1.2
Area ratio	2.56
Convergent angle	15
Divergent angle	0.5
Inlet diameter	21 mm
Outlet diameter	10 mm
Throat diameter	9.9 mm
Convergent length	20 mm
Divergent length	8.6 mm
Duct diameter	16 mm
Duct length	Varies from 1D to 6D

Next, the area ratio for the model is expressed by the equation below.

$$Area\ ratio = \frac{\frac{\pi D_p^2}{4}}{\frac{\pi D_n^2}{4}} = \frac{D_p^2}{D_n^2} = \frac{16^2}{10^2} = 2.56$$

Dp is the diameter of the duct, and Dn is the diameter of the nozzle.

3.3 Simulation Model

The axisymmetric convergent-divergent nozzle model configurations with annular ribs were simulated using ANSYS Workbench 2023 Design Modeler. Figure 5 below illustrates an example of the geometry, with the ribs located at 0.5D and L/D = 1.

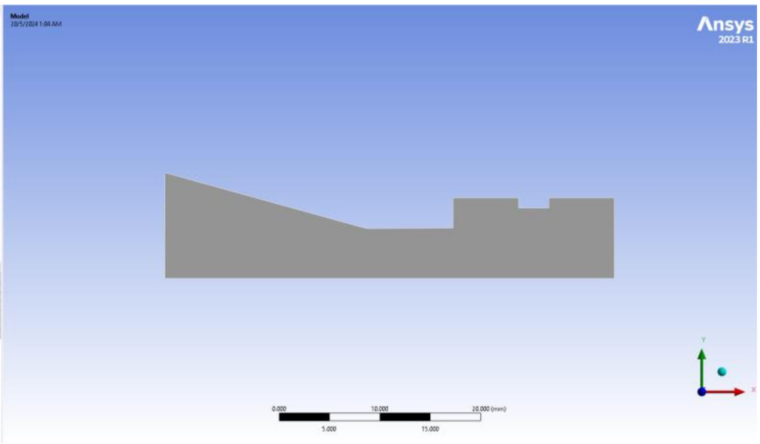

Fig. 5. Display of nozzle and duct configuration in ANSYS Fluent

3.4 Meshing and Analysis

The Automatic Method is applied to all quads as indicated to start the meshing process. The element size, 0.3 mm, has been standardized to all C-D nozzle dimensions. The meshing results on the geometry are demonstrated in Figure 6, and it applies to all L/D variations with the same mesh density.

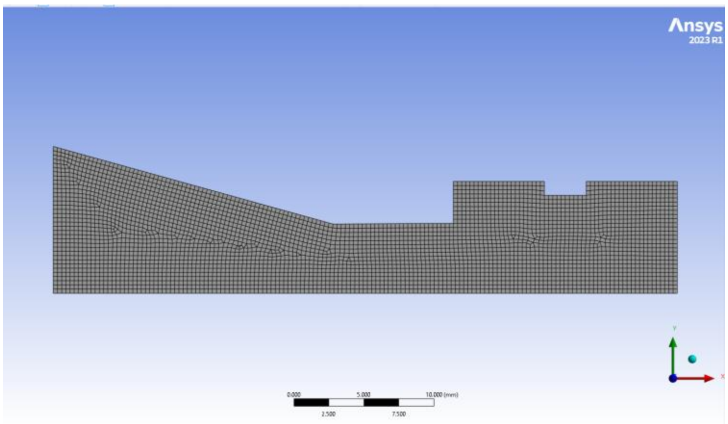

Fig. 6. Meshing density for 0.3 mm element sizes

The initial stage of numerical modelling involves the selection of a suitable mathematical model, encompassing governing equations, boundary conditions, mesh quality, and a numerical method to solve the governing equations simultaneously. Next, a numerical method is chosen to solve the governing equations. Despite the computational method's inability to precisely represent physical events, it offers valuable insights into flow behavior and has been heavily relied upon for many years. Therefore, it is imperative to carefully choose features that accurately reflect the behavior of the flow. This study analyzes the assumptions to achieve a satisfactory compromise with the accurate physical reality. The assumptions and features discussed in this study are as follows

i. The flow is a steady-state-two-dimensional flow due to the flow being symmetric along the flow direction.
ii. The velocity flow is considered turbulent because the viscous dissipation effects are considerable.
iii. The fluid is compressible, and its viscosity is a function of temperature.
iv. The flow exits from the duct at ambient atmospheric pressure.

Before commencing the simulation calculation, specific preparations are necessary within the CFD Simulation Setup. These preparations include the general configurations, models, materials, boundary conditions, initialization, and calculation. Under the general section, the solver type must be adjusted to density-based, and the time setting must be established as steady. In the 2D space category, the axisymmetric option is selected, ensuring that the analysis of the experiment addresses the resolution of a 2D axisymmetric problem. The energy equation for the energy model is activated. In the viscous model panel, the k-epsilon model is selected, and the standard variant is chosen. Standard wall functions are applied for the near-wall treatment. In selecting the material, fluid air is chosen, with the density set to the ideal gas and the viscosity governed by the Sutherland Law. Other properties, including specific heat, thermal conductivity, and molecular weight, are set to constant values. The boundary conditions for the nozzle inlet and the Gauge Total Pressure (GTP) can be found by deriving the NPR formula below. The GTP for all other zones must be set at 0.

$$NPR = \frac{GTP + P_{atm}}{P_{atm}}$$

Next, the solution initialization is set to hybrid initialization, and the number of iterations is set to 10000.

3.5 Mesh Generation and Independence Check

The meshing of the geometry plays a crucial role in the stability and accuracy of numerical computation. The result computing time and the results' accuracy depend on the mesh density, which also means the element's size. The FEA theory states that a Finite Element Model with fine-meshed elements yields high accuracy, but the process may take more computing time. The fine mesh may be used only when high accuracy and precision are required. The Finite Element Model with coarse mesh may simulate the results in a short computing time, but the results obtained may not be accurate compared to the fine mesh FE model. Choosing the appropriate mesh and element size is necessary to get the FEA results with high accuracy with minimum possible commuting time.

A quality mesh is the first step in ensuring that the computational fluid dynamics solver generates the correct solution while using as few processing resources as possible. When defining mesh quality, the first step is straightforward: if a mesh does not converge or produce a result, it is a bad mesh.

However, things become more complicated from there, as there are decent and even better meshes. Perhaps the essential feature is how accurately the CFD solution matches real-world occurrences.

This project involved the refinement of an unstructured rectangular mesh. Grid sizes are adjusted to provide sufficient accuracy and convergence. The same geometry is utilized to determine mesh independence. Five alternative element sizes and nodes are simulated. Each element size was simulated using different NPR values ranging from 1.5 to 5. The element size and its corresponding number of elements are shown in Table 5.

Table 5
Different element sizes with their properties based on the same geometry model

Element Size	Number of Element	Number of Nodes
Coarse	1251	1354
Fine	3277	3452
Finest	78167	78988

The mesh independence check's goal is to determine the appropriate element size. Higher NPR requires more rounds and takes longer to compute. Selecting the proper element size can achieve higher precision with less computation time. Table 5 shows that the finer the element size, the denser the mesh. For the finest element sizes, there are more elements and nodes. The percentage difference between element sizes with the same NPR and design geometry must be less than 20% to determine the appropriate element size for meshing. In general, 10k iterations are sufficient for the solutions to converge; however, 20k iterations ensure that the solutions converge with high correctness.

Table 5 shows various element sizes, the number of elements, and the number of nodes. Figure 7 shows that the chosen grid size is the finest, with approximately 78988 nodes and 78167 elements. This is because the variation in base pressure ratio between finer and finest grid sizes is less than 5%. If the element size is reduced while the number of elements increases, the number of iterations exceeds 10,000, and the computational time increases. As a result, the best element size equals the ideal grid size.

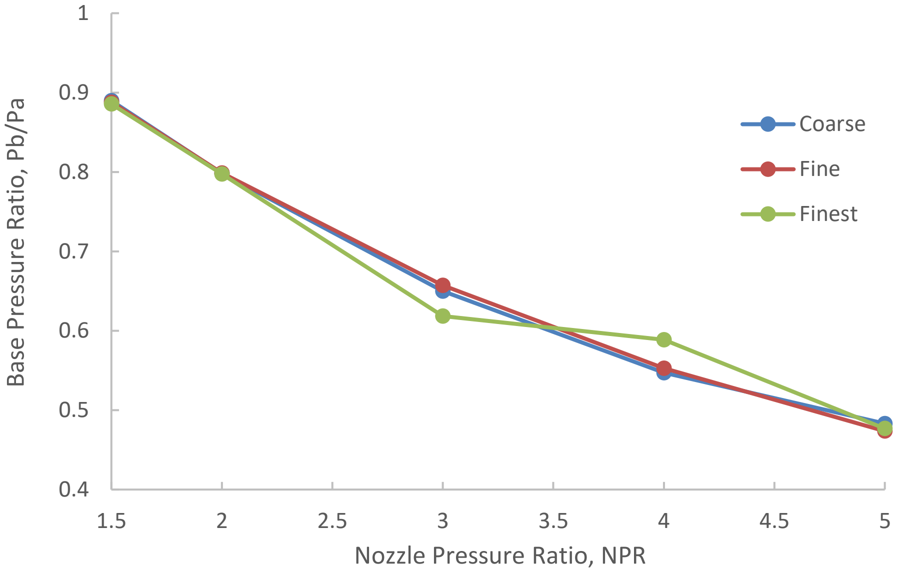

Fig. 7. Three different element sizes having converged values

3.6 Validation of Previous Work

According to Rathakrishnan [46], the prior work was performed at aspect ratios of 3:3, 3:2, and 3:1; an area ratio of 6.25; L/D ranging from 1 to 6; pressure ratios of 1.141, 1.295, 1.550, 1.707, and 2.458; and nozzle exit Mach numbers of 0.44, 0.62, 0.82, 0.91, and 1.0. However, in a prior publication by Rathakrishnan [46], the result from Figure 8 with NPR (P01/Pa) 2.458 and models with control in the form of ribs with 3:2 and 3:3 aspect ratios was chosen to be compared to the current work. The simulation is supported by Radhakrishnan's [46] experimental work, which used five ribs positioned at equidistant intervals in the duct, as illustrated in Figure 2. The results of base pressure fluctuation with NPR of 2.458 and L/D ranging from 2 to 6 are obtained. The study is repeated to validate the numerical results of a model with control over different rib aspect ratios.

Figure 8 demonstrates the current and earlier studies' base pressure ratio data curves [46]. The experimental values were denoted by dotted lines, while the simulation results obtained using ANSYS Fluent were represented by straight lines. The current numerical work had a percentage error of less than 10% compared to the earlier experimental work. As a result, the current work fell within the acceptable range. The curves followed the same pattern; each point was close to the next. As a result, based on the table and graph described before, the validation of the current work was successful.

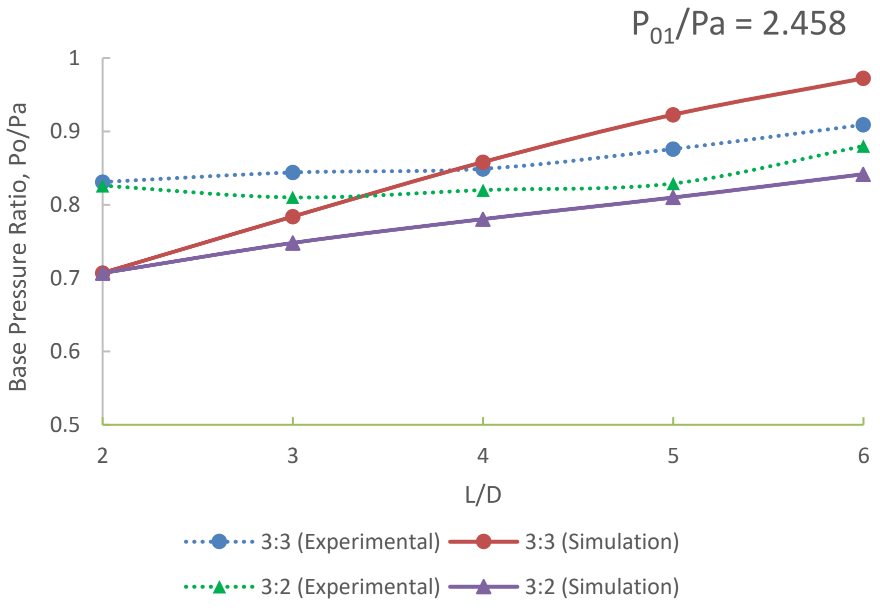

Fig. 8. Validation of previous work by Rathakrishnan [46]

4. Results and Discussions

This study aims to assess the nozzle flow from a converging-diverging nozzle and the effectiveness of the ribs of different sizes and locations in a suddenly expanded duct at supersonic Mach number 1.2.

4.1 Selected Pressure Contours: CD Nozzle with Sudden Expansion Duct Having Ribs

The figures in the document reveal critical insights into the behavior of high-speed flows as they interact with ribs of varying configurations within a suddenly expanded duct. Each configuration provides unique insights into how passive ribs can manipulate flow dynamics.

Figure 9 to Figure 11 show pressure contours for ribs with aspect ratios of 3:1, 3:2, and 3:3, respectively, all located 0.5D from the base wall. At this proximity to the expansion, ribs immediately influence the flow by inducing shock waves and separation bubbles. The varying aspect ratios demonstrate how the thickness of the rib can either amplify or dampen these effects. Thicker ribs (3:1) tend to cause more pronounced flow separation, as evident in Figure 1, leading to larger recirculation zones, which can be detrimental by increasing pressure drag but are beneficial for mixing applications. Conversely, thinner ribs (3:3 in Figure 3) might result in less obstruction to the flow, reducing recirculation and potentially leading to a more streamlined flow post-expansion.

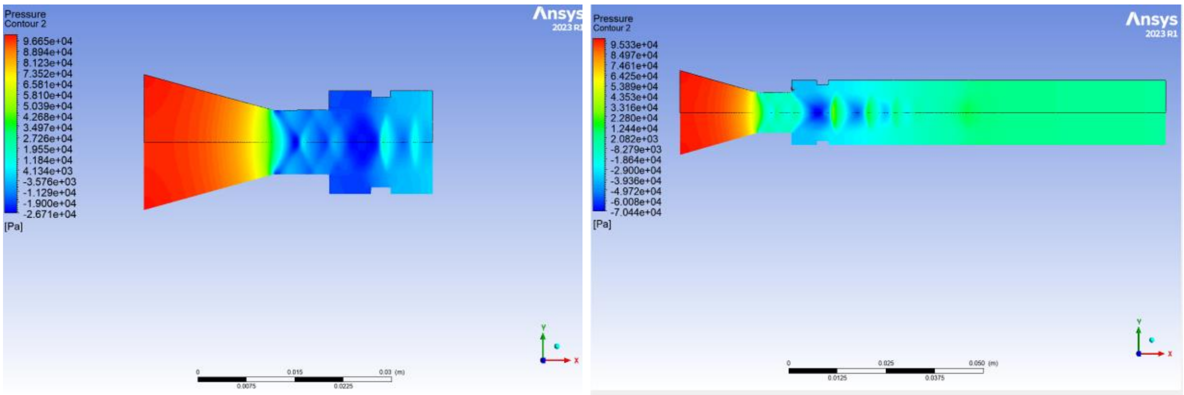

Fig. 9. Contours result of L/D 1 and 6 at NPR 2

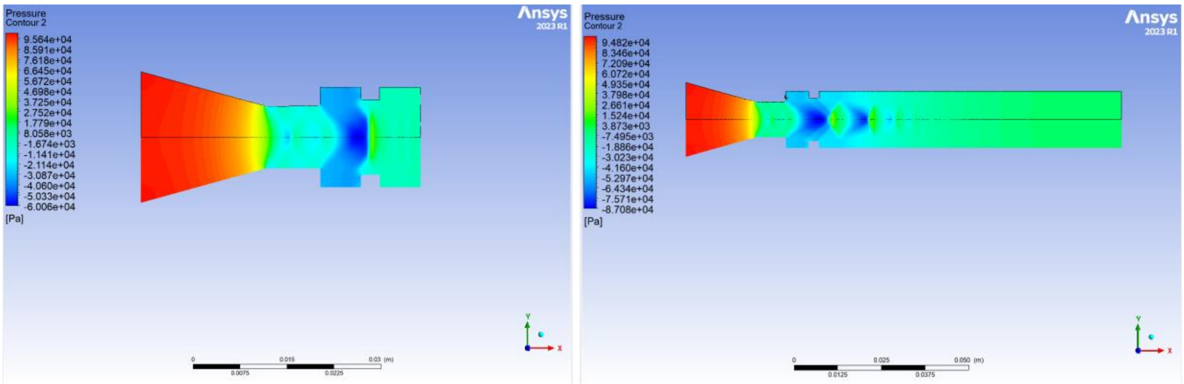

Fig. 10. Contours result of L/D 1 and 6 at NPR 2

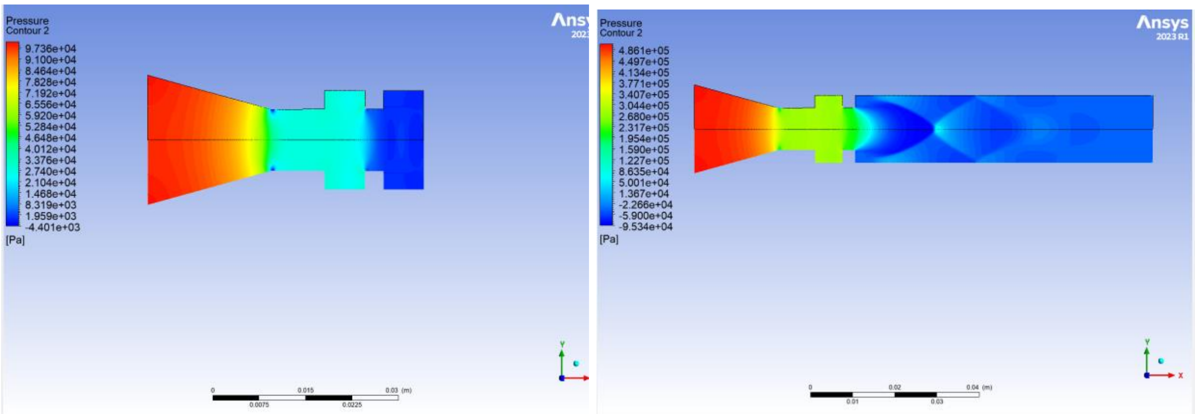

Fig. 11. Contours result of L/D 1 and 6 at NPR 2

Figure 12 to Figure 14, with ribs of aspect ratio 3:1 at 1D to 2D locations, show how increasing the distance from the base wall affects the flow. As the rib is placed further away, the flow can develop more fully before encountering the obstruction. This can reduce the abruptness of flow separations and improve pressure recovery downstream, as indicated by smoother contours in these figures. The influence on pressure recovery is critical for efficiency, particularly in propulsion systems where energy loss minimization is vital.

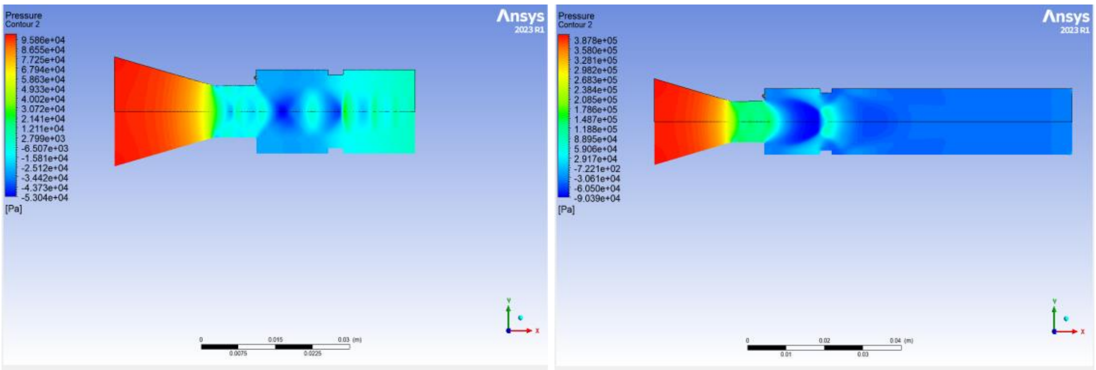

Fig. 12. Contours result of L/D 1 and 6 at NPR 2

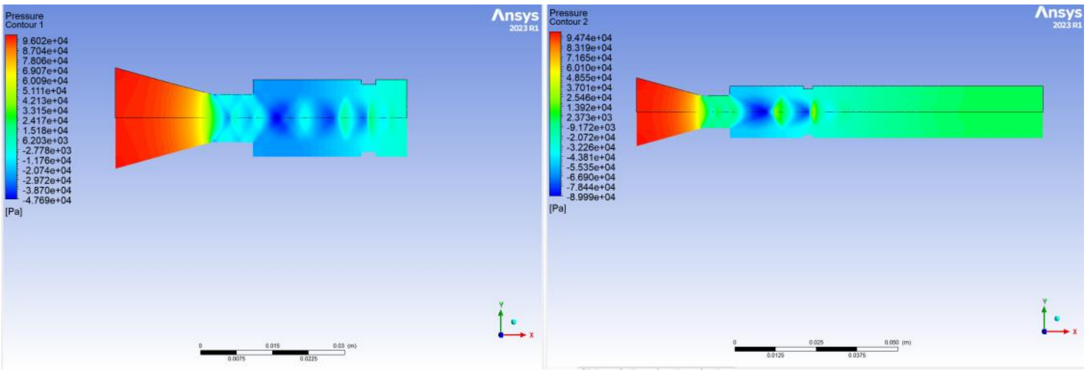

Fig. 13. Contours result of L/D 1 and 6 at NPR 2

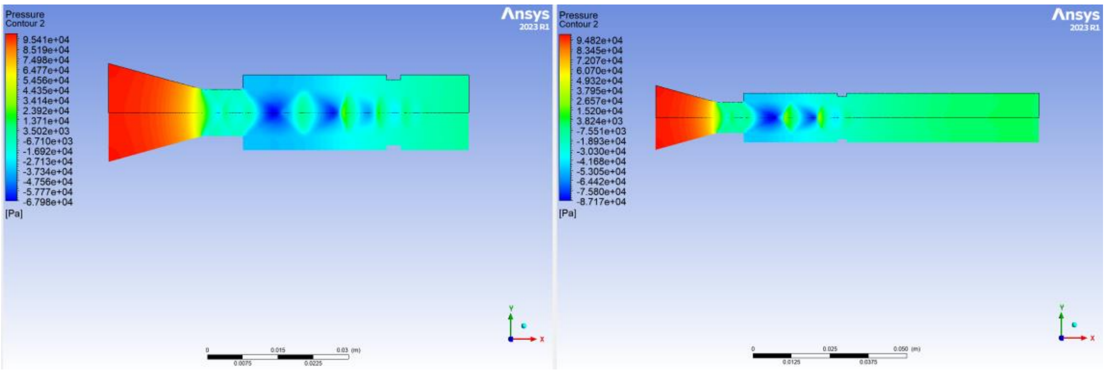

Fig. 14. Contours result of L/D 3 and 6 at NPR 2

Figure 15 and Figure 16, where the rib is located even further at 3D and 4D, illustrate an advanced stage of flow interaction. The duct's length allows for a fully developed turbulent profile before the flow hits the rib. This can be crucial for applications requiring stable flow conditions at the exit of the expansion, as the disturbances induced by the ribs are better dissipated.

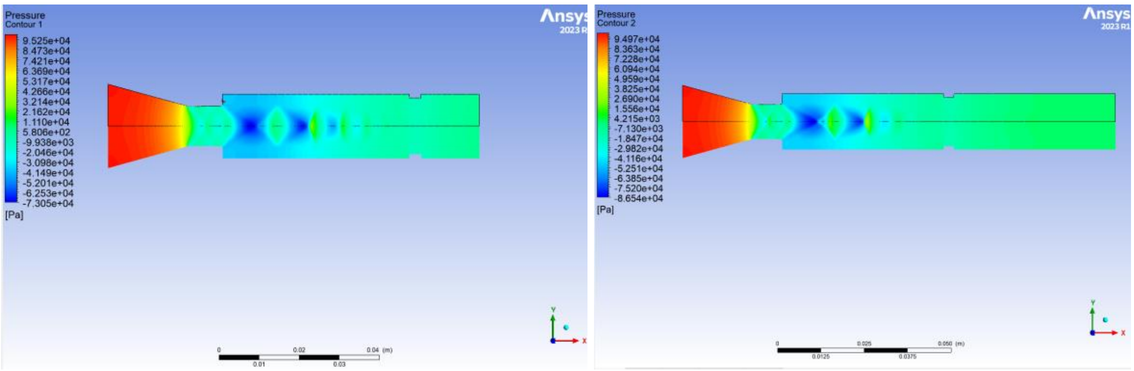

Fig. 15. Contours result of L/D 4 and 6 at NPR 2

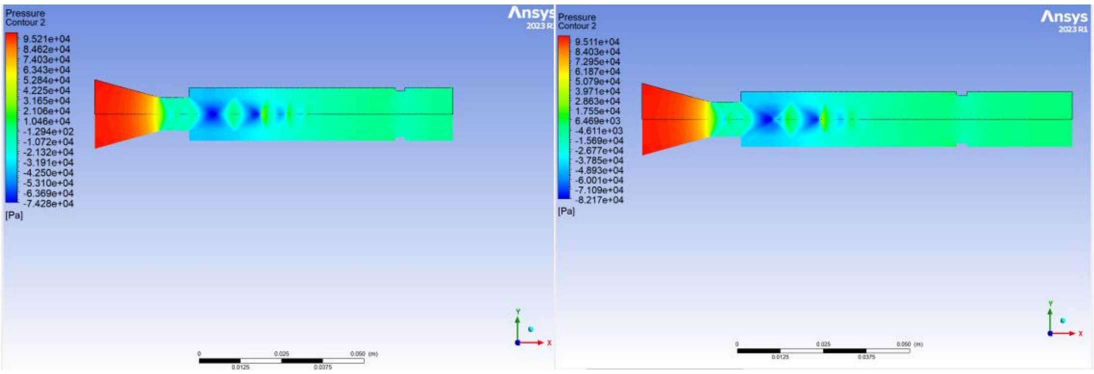

Fig. 16. Contours result of L/D 5 and 6 at NPR 2

Figure 17 to Figure 26, where ribs with aspect ratios of 3:2 and 3:3 are tested at distances of 1D to 4D, continue to explore these dynamics. The increasing aspect ratio at these positions shows how a wider rib can influence the flow. Particularly in longer ducts (evident in higher figure numbers), the ribs help control the boundary layer development and flow separation, which is crucial for maintaining desired flow characteristics over extended distances.

The nozzle pressure ratio (NPR), while constant at 2 for all configurations, plays a crucial role in defining the overall energy state of the flow entering the duct. Higher NPRs generally increase the total pressure across the system, which can amplify the effects of ribs in controlling the flow due to higher energy interactions at the rib boundaries. Each figure provides a detailed examination of how ribs affect high-speed flow in a duct, showing that the location and size of ribs are crucial for managing flow separation, pressure recovery, and energy efficiency. The rib parameters must be aligned with the specific aerodynamic goals, such as minimizing energy losses in propulsion systems or enhancing mixing in combustion applications.

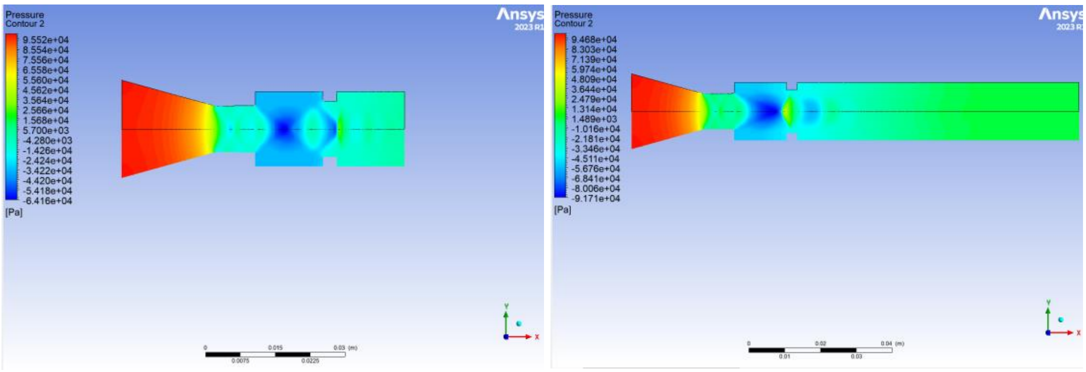

Fig. 17. Contours result of L/D 2 and 6 at NPR 2

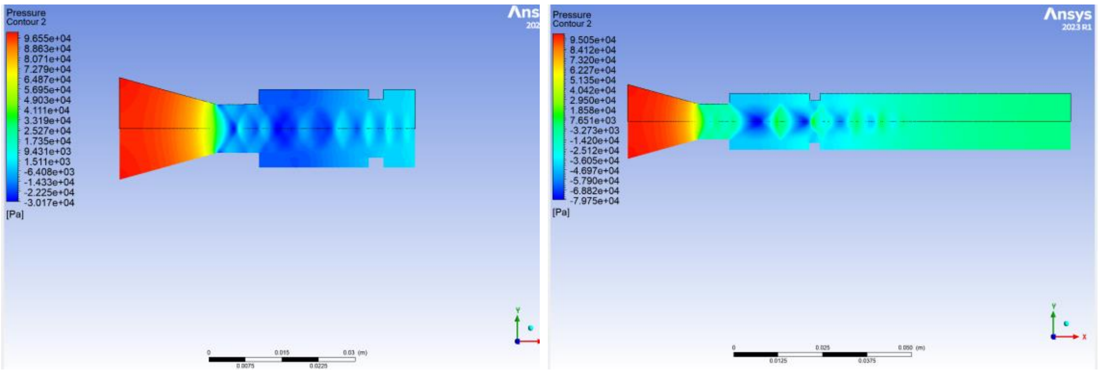

Fig. 18. Contours result of L/D 2 and 6 at NPR 2

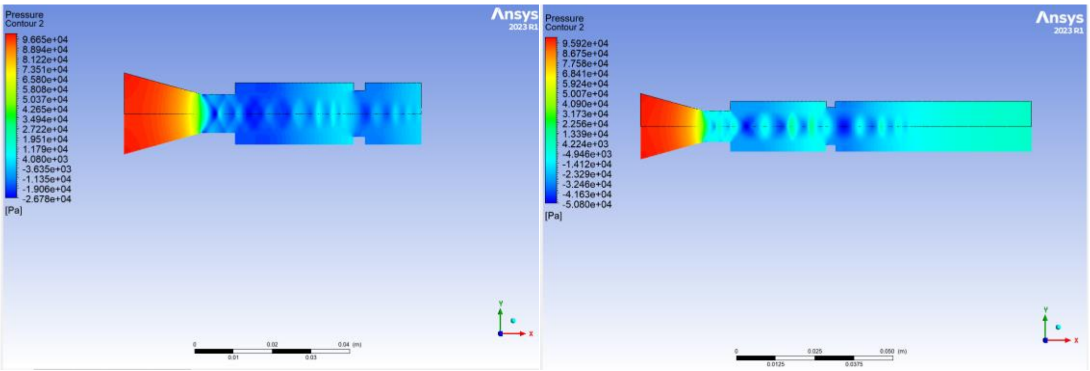

Fig. 19. Contours result of L/D 3 and 6 at NPR 2

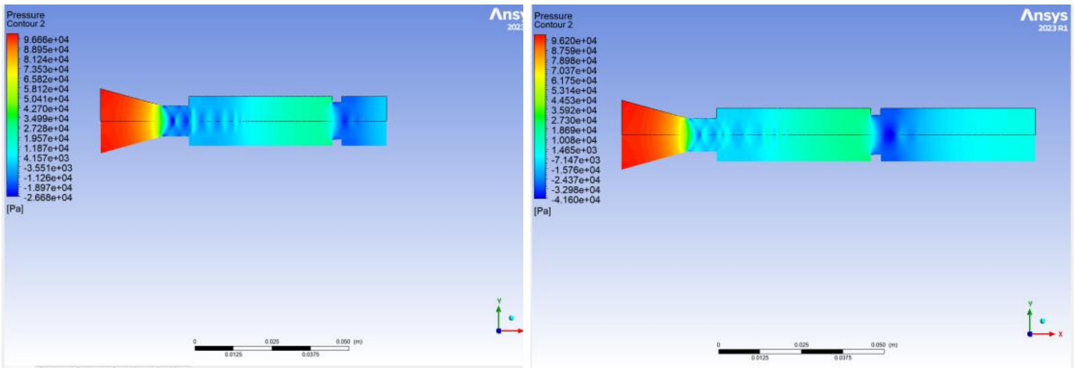

Fig. 20. Contours result of L/D 4 and 6 at NPR 2

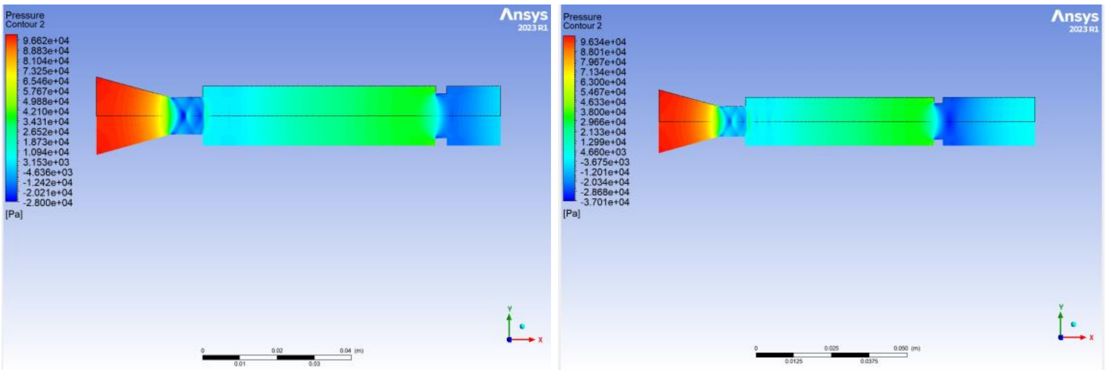

Fig. 21. Contours result of L/D 5 and 6 at NPR 2

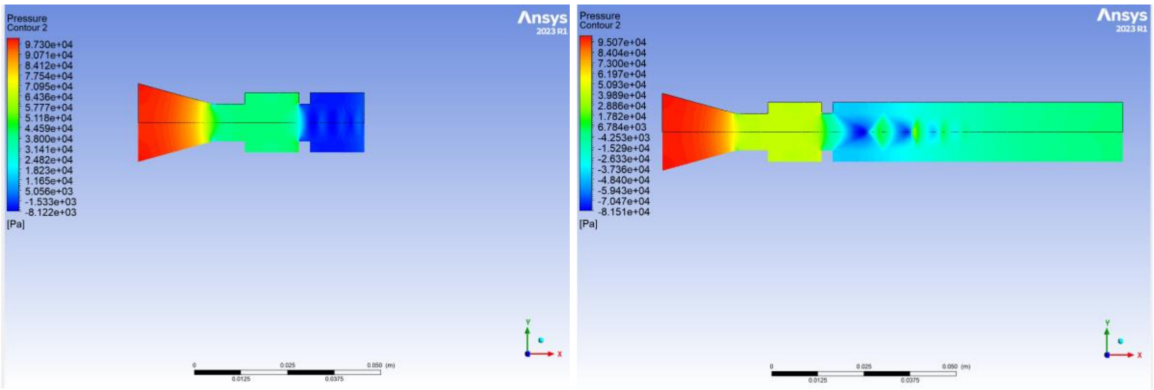

Fig. 22. Contours result of L/D 2 and 6 at NPR 2

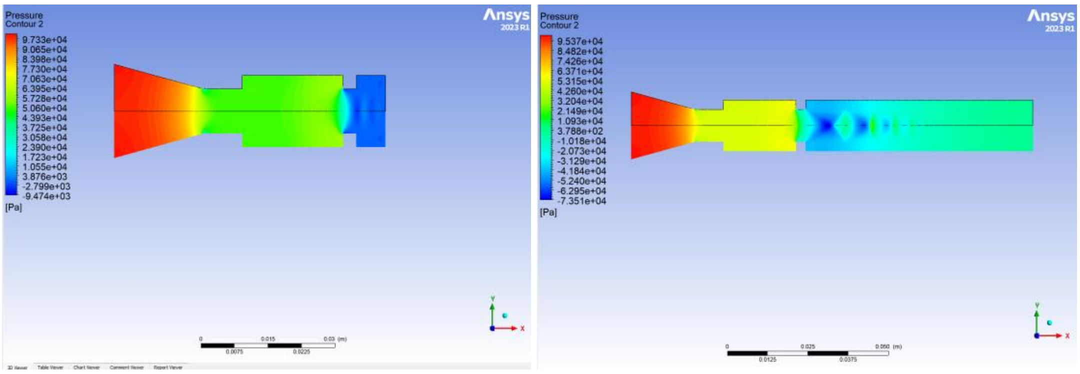

Fig. 23. Contours result of L/D 2 and 6 at NPR 2

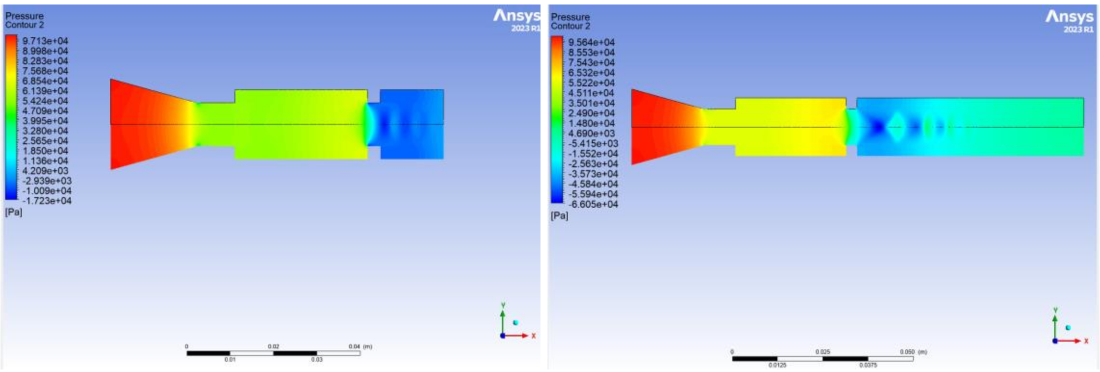

Fig. 24. Contours result of L/D 3 and 6 at NPR 2

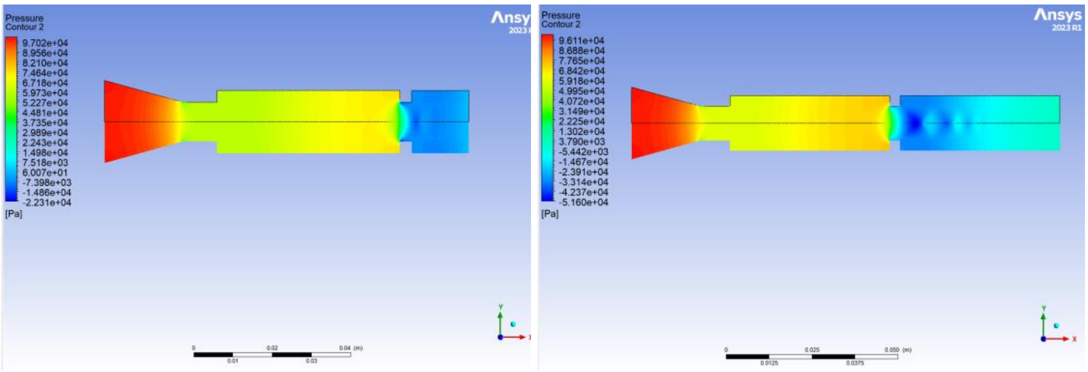

Fig. 25. Contours result of L/D 4 and 6 at NPR 2

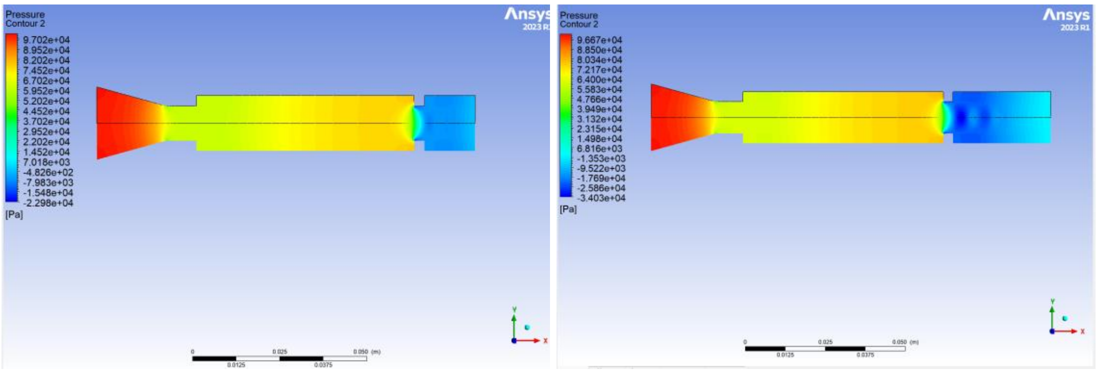

Fig. 26. Contours result of L/D 5 and 6 at NPR 2

4.2 Base Pressure (Pb/Pa) vs Nozzle Pressure Ratio Plot (3:1 RIBS and 3:2 RIBS)

Initially, the base pressure extracted from the Ansys file, gauge pressure, is converted to absolute pressure by adding ambient atmospheric pressure. Later, this absolute pressure is made non-dimensional by dividing the absolute pressure with ambient atmospheric pressure.

The Mach number of the present study is M = 1.2, and the NPR at the correct expansion is 4.2. This study conducted simulations for NPRs 2, 3, 4, 5, and 6. The level of expansion (Pe/Pa) at these NPRs is 0.83, 1.24, 1.65, 2.06, and 2.5. While scanning the literature, the researchers working in flow control concluded that the control becomes active or passive effective once the nozzles flow under a favorable pressure gradient. This means that the nozzles are under-expanded, and the control employed becomes effective. Hence, there is a need to analyze the results to keep these findings in mind.

Base pressure distribution with nozzle pressure ratio (NPR) for ribs with aspect ratios 3:1 and 3:2 for various duct lengths is shown in Figure 27. From Figure 27(a) to Figure 27(f), it is evident that the base pressure values are oscillatory, and there are marginal variations in the base pressure values for more significant duct lengths. This trend may be due to the small duct lengths, namely L/D = 1 and 2, where the ambient pressure will influence flow in the duct. Figure 27(a) shows that the base pressure continues to decrease till NPR = 4, and later, there is a progressive increase in the base pressure. When the rib of 3:1 is employed as passive control, there is an increase in the base from NPR = 3 onwards. However, for ribs with a 3:2 aspect ratio, there is an increase in the base pressure right from NPR = 2. Also, it is seen that the flow pattern for L/D = 1 is quite different from the other L/Ds from 2 to 6. There are two reasons for this pattern. First is the small duct length, and second is the locations of the ribs at 0.5D. When flow exits from the nozzle, it faces expansion waves and a separated shear layer coupled with the strong influence of the atmospheric pressure.

When we look at the base pressure results for other L/Ds from 2 to 6, the decrease in the base pressure gets arrested at NPR = 3 instead of NPR = 4 for the without-control case, and the rest of the trends are almost the same with a marginal change in the magnitude of the base pressure.

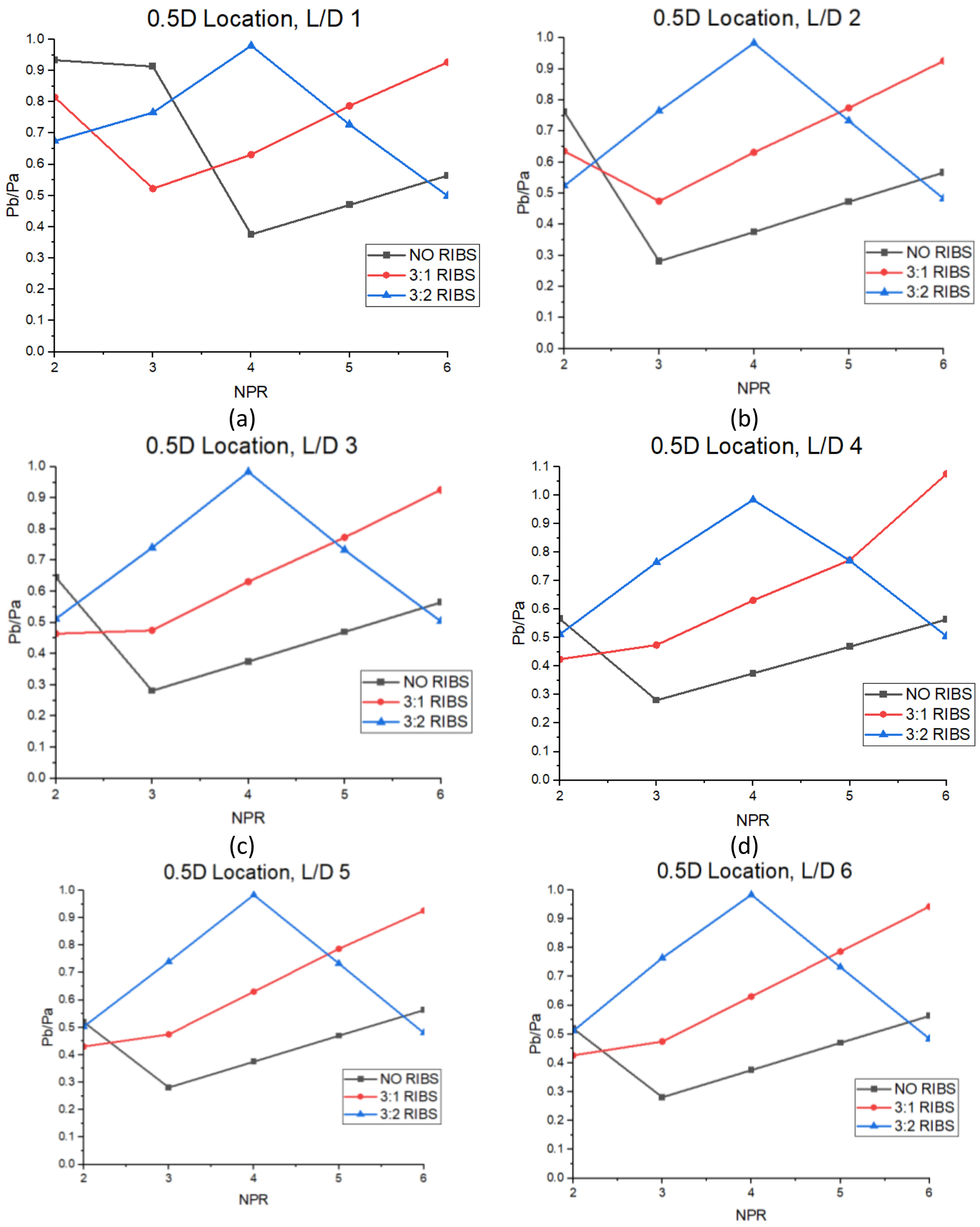

(a) (b)

(c) (d)

(e) (f)

Fig. 27. The base pressure ratio variations with NPR rib at 0.5D

Figure 28(a) to 28(e) show the base pressure variation with NPR for two ribs of aspect ratios 3:1 and 3:2 for enlarged duct lengths from 2D to 6D when ribs are placed at 1D locations. As discussed earlier, in the absence of control, the decreasing trend in the base pressure is reversed from NPR = 3 and above. The same trend is seen here even though the location of the ribs is fixed at 1D. When the control is employed, it increases base pressure from NPR = 3 and above for ribs with an aspect ratio of 3:1. However, for ribs with an aspect ratio of 3:2, control does not show its impact at NPR = 2, but from NPR = 3 and above there is a continuous rise in the base pressure. Similar trends are seen at the duct length = 2D and 3D. It is also seen that for duct lengths, 4D, 5D, and 6D oscillations in base pressure are seen due to the combined effect of the rib's location, level of expansion, and the duct size, which influences the flow inside the duct. For the highest duct length, the base pressure is 20% more than the ambient pressure. The results show that flow in the nozzle attains critical conditions, and the flow becomes under-expanded for NPR more than two. These results reiterate that active or passive control becomes effective whenever the nozzles flow under a favorable pressure gradient.

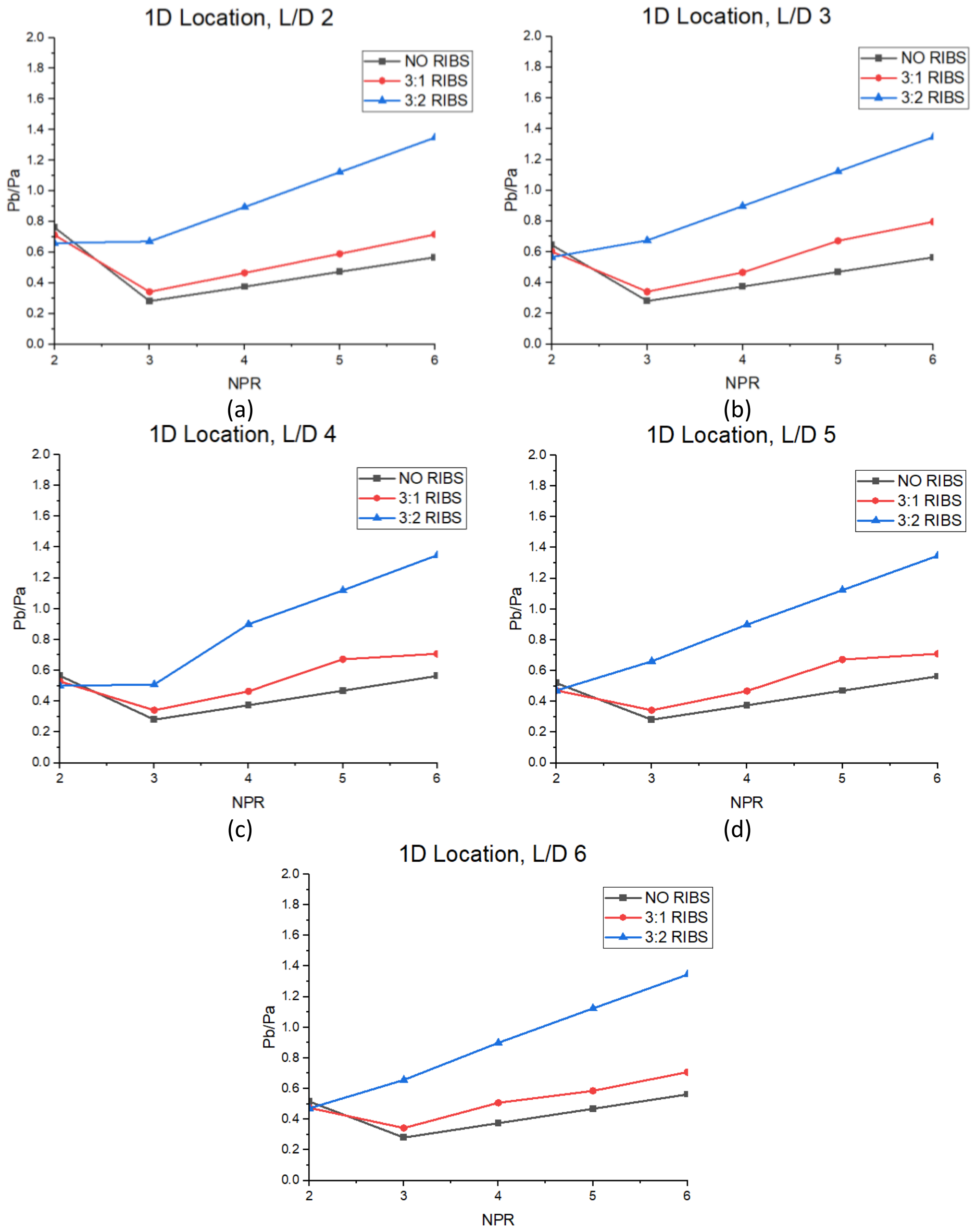

(a) (b) (c) (d) (e)

Fig. 28. The base pressure ratio variations with NPR for rib at 1D

Figure 29(a) to Figure 29(e) show the base pressure variation with NPR for two ribs of aspect ratios 3:1 and 3:2 for enlarged duct lengths from 2D to 6D for rib locations of 1.5D. As discussed earlier, in the absence of control, the decreasing trend in the base pressure is reversed from NPR = 3 and above. Also, it is seen that there is a significant decrease in the base pressure from 0.7 to 0.2, but with an increase in the NPR and attaining a maximum value of 0.6 at the highest NPR of simulation. The same trend is seen here even though the location of the ribs is fixed at 1.5 D. When the control is employed. It increases base pressure from NPR = 3 and above for ribs with an aspect ratio of 3:1. The figure shows that base pressure values remained in the range from 0.7 to 0.85. However, for ribs with an aspect ratio of 3:2, control does not show its impact at NPR = 2, but from NPR = 3 and above, there is a continuous rise in the base pressure, and the base pressure values 60% more than the ambient pressure. Similar trends are seen at the duct length = 3D and 4D, except that of marginal variation in the magnitude of the base pressure values. It is also seen that for duct lengths, 4D, 5D, and 6D oscillations in base pressure are seen due to the combined effect of the rib's location, level of expansion, and the duct size, which influences the flow inside the duct. For the highest duct length, the base pressure is 20% more than the ambient pressure. These trends are attributed to the expansion level, rib sizes, and locations.

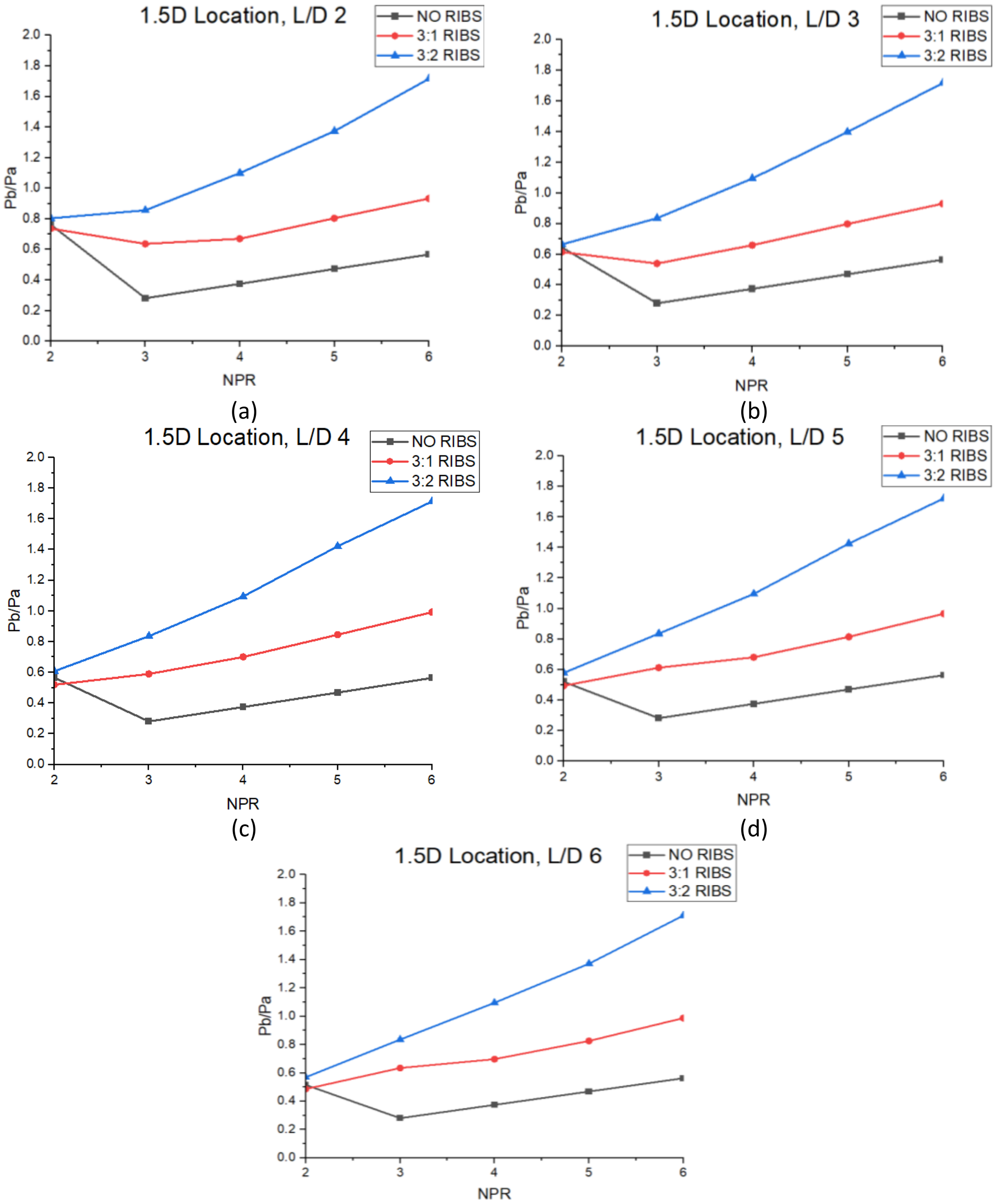

(a) (b)

(c) (d)

(e)

Fig. 29. The base pressure ratio variations with NPR for rib at 1.5D

Figure 30(a) to Figure 30(e) presents the base pressure results for two ribs of aspect ratio 3:1 and 3:2 for rib location of 2D for NPRs in the range 2 to 6. Results for L/D = 3 when ribs are located at 2D are shown in Figure 30(a). The base pressure results for 2D rib location show that for rib with an aspect ratio of 3:2, there is a progressive increase in the base pressure, whereas, for rib with a 3:1 aspect ratio and in the absence of control, there is a decrease in the base pressure till NPR = 3 for both the cases and control becomes effective. Base pressure progressively assumes higher values with increased NPR and, hence, the under-expansion level. The physics behind this trend is that at NPR = 3, the nozzle is under-expanded, and the level of under-expansion is 1.24 (i.e., Pe/Pa = 1.24).

Regarding ribs with an aspect ratio of 3:2, there is a continuous increase in the base pressure right from NPR = 2. When the rib height is 2 mm, the exiting flow from the nozzle has no space to create suction, and the base pressure values at NPR = 6 are twice the ambient atmospheric pressure. Similar results are shown in Figure 31(b) to Figure 31(e) for duct lengths 4D, 5D, and 6D. It is seen that flow has attained a steady state, and higher duct lengths are unable to influence the flow field inside the duct. Hence, safely, we can say that flow in the duct is established and remains attached to the duct.

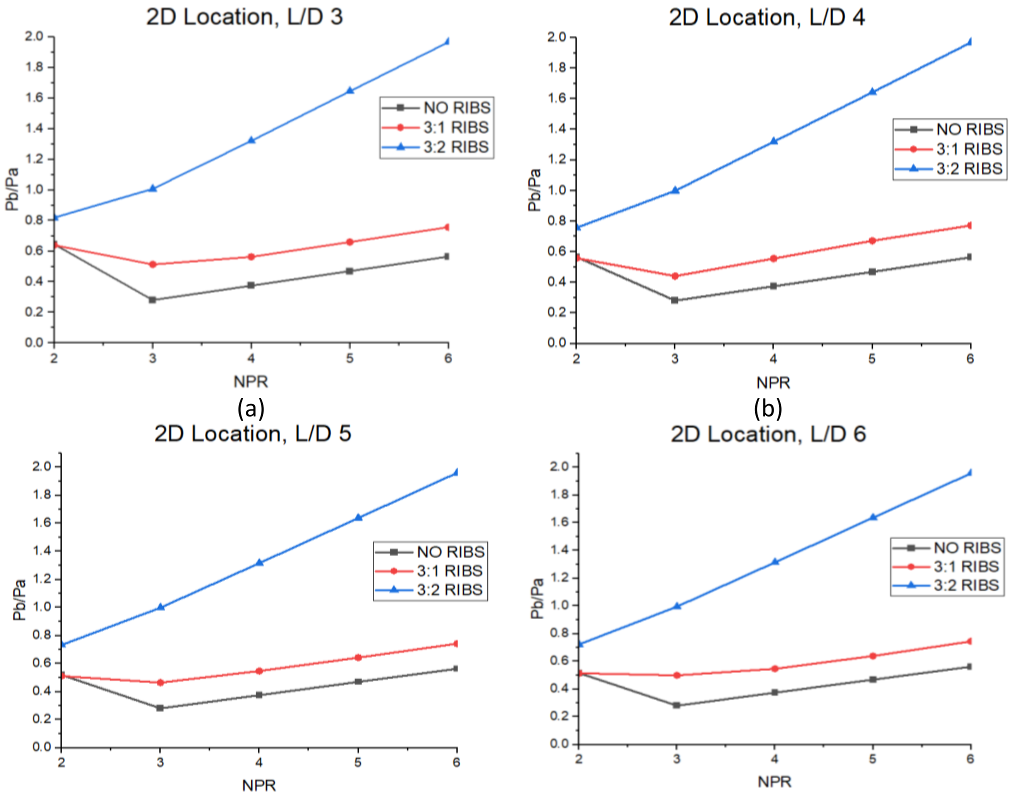

(a) (b)

(c) (d)

Fig. 30. The base pressure ratio variations with NPR for rib at 2D

Base pressure results as a function of NPR, and for ribs, the aspect ratio is 3:1 and 3:2 for 3D locations of the ribs, as shown in Figure 31(a) to Figure 31(c). These results differ from the previous case, where the rib was located at 2D. Regarding the rib of aspect ratio 3:2, results show that the base pressure values are nearly three times the atmospheric pressure at NPR = 6. In contrast, when ribs were located 2D for the same level of expansion, the base pressure was two times the ambient pressure. When we look at the base pressure pattern for a rib with an aspect ratio of 3:1, there is a sudden drop in the base pressure till NPR = 3; later, there is an increase in the base pressure. However, the variation of the base pressure is not linear. Some waviness in trend is seen; it is more prominent for the rib of aspect ratio 3:1 instead of rib 3:2. To understand the flow's physics, one must analyze the results critically. The duct diameter is 16 mm; hence, the step height is 3mm at the top and bottom from the axis of symmetry. Because of the small step, the reattachment length seems to be small. The results show that the reattachment point is around 1 D (i.e., 16 mm) from the base. After the reattachment point again, the boundary layer will be formed, and through the shear layer, flow development will take place, and the wall duct pressure recovery will also occur. Under these circumstances, when the ribs are placed beyond the reattachment point, the vortices created by the sharp corner will interact with the boundary layer depending upon the height of the ribs. When rib height is small, for instance, in the case of the aspect ratio 3:1, where the rib height is just 1 mm, it seems the rib is inside the boundary layer. The viscous forces are concentrated inside the boundary layer, and the flow is compressible, viscous, and rotational. Because of this situation, the rib is also located inside the boundary layer, generating vortices from the top two sharp corners, resulting in the oscillatory nature of the flow. This may be why base pressure oscillates when a rib of 1 mm is placed at a 3D location.

Similar results are seen for other duct lengths L = 5D and 6D in Figure 31(b) to Figure 31(c). The increase in the duct length does not impact the base pressure values, which indicates that the flow has stabilized and is steady and independent of the duct length.

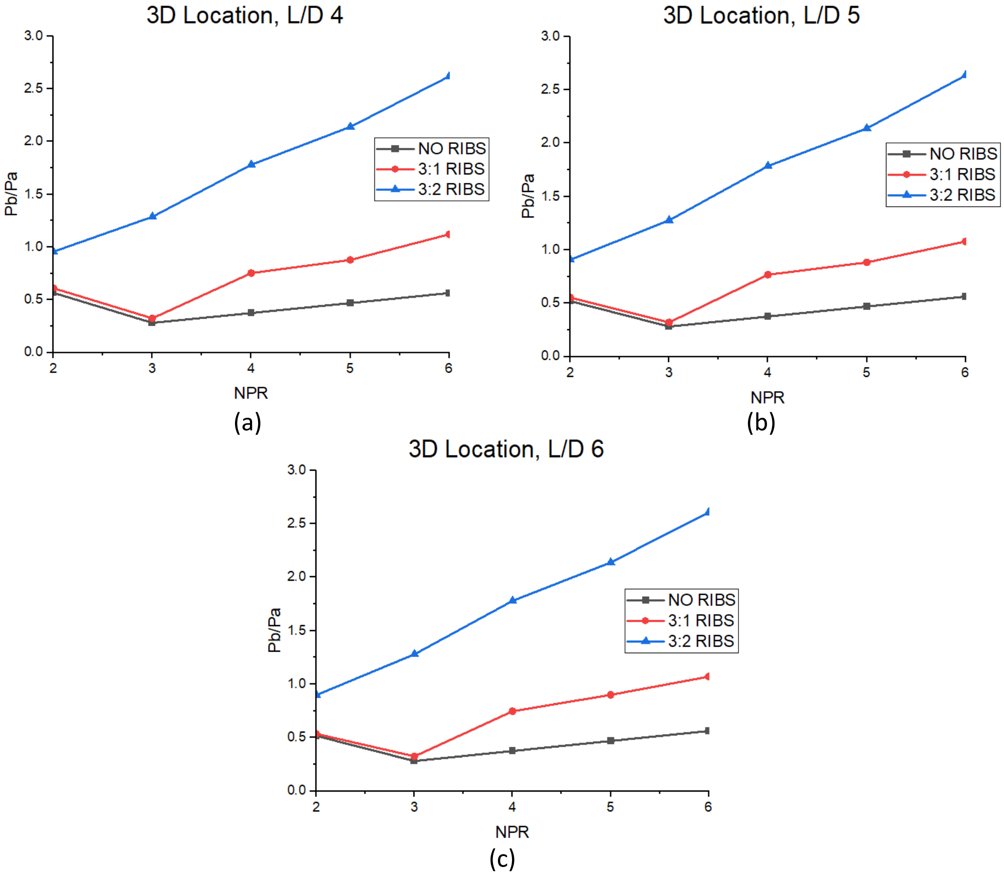

(a) (b)

(c)

Fig. 31. The base pressure ratio variations with NPR for rib at 3D

Figure 32(a) to Figure 32(b) show the findings of the present study when ribs are placed at 4D locations with aspect ratios of 3:1 and 3:2. The results at 4D locations are different from the base pressure results when ribs are located at 3D. However, these results are nearly identical to those when ribs are located from 0.5D to 2D. As discussed earlier, there is a decrease in the base pressure for the plain duct up to NPR = 3. Later, there is an increase in the base pressure.

Meanwhile, for rib aspect ratio 3:1, there is a linear rise in the base pressure, and base pressure is nearly equal to the atmospheric pressure, in contrast to the results for rib aspect ratio 3:2 right from NPR = 2, the starting base pressure values are equal to the atmospheric pressure and with an increase in the NPR as high as the base pressure values are three bar. The change in the base pressure values is due to the location of the ribs and the considerable duct length exposed to the ambient atmosphere. Here, the ambient pressure impacts considerably the flow field inside the enlarged duct. The reattachment seems to be around 1D or 2D. When ribs are located at 4D and duct lengths are 5D and 6D, the rib location is far from the shear layer, resulting in less interaction with the viscid layer. For this duct location and length, the influence of the atmospheric pressure may be more significant than that of the other rib position.

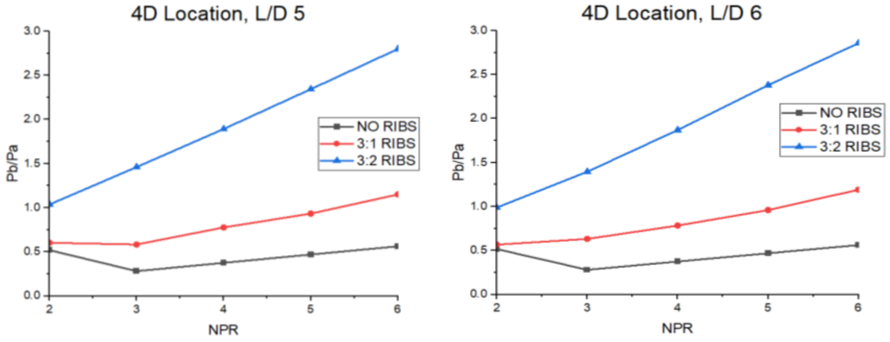

(a) (b)

Fig. 32. The base pressure ratio variations with NPR for rib at 4D

4.3 Base Pressure (Pb/Pa) vs Nozzle Pressure Ratio Plot (3:3 RIBS)

Base pressure results for various duct lengths from L = 1 to 6D when the rib is placed at 0.5D are shown in Figure 33(a) to Figure 33(f). The results for L/D = 1 show a different pattern due to the small duct length and flow field inside the duct being influenced by the ambient atmosphere for NPR = 2 to 4 in the absence of ribs. When nozzles are highly under-expanded, the influence of the atmosphere is reduced, as seen in Figure 34(a). When ribs of aspect ratio 3:3 are employed, it is seen that the base pressure values are 25% more than the ambient pressure values, and for NPR = 6, base pressure values are 3.7 bar, which is an outstanding achievement.

The following factors are responsible for such a high base pressure value: the most critical one is the height of the rib, the secondary vortices at the two sharp corners, which will interact with the base vortices, weakening the base vortices and resulting in high base pressure values. Similar results are seen for duct lengths 2D to 6D, except for base pressure results without control. In the case of the without control case, the marginal oscillations that were there for L/D = 1 are absent as the duct length is enough for the flow to get attached to the duct wall, and the impact of the ambient pressure is minimal. However, when the control is employed, there is a considerable increase in the base pressure, and this pattern sustains all duct lengths right from 1D to 6D.

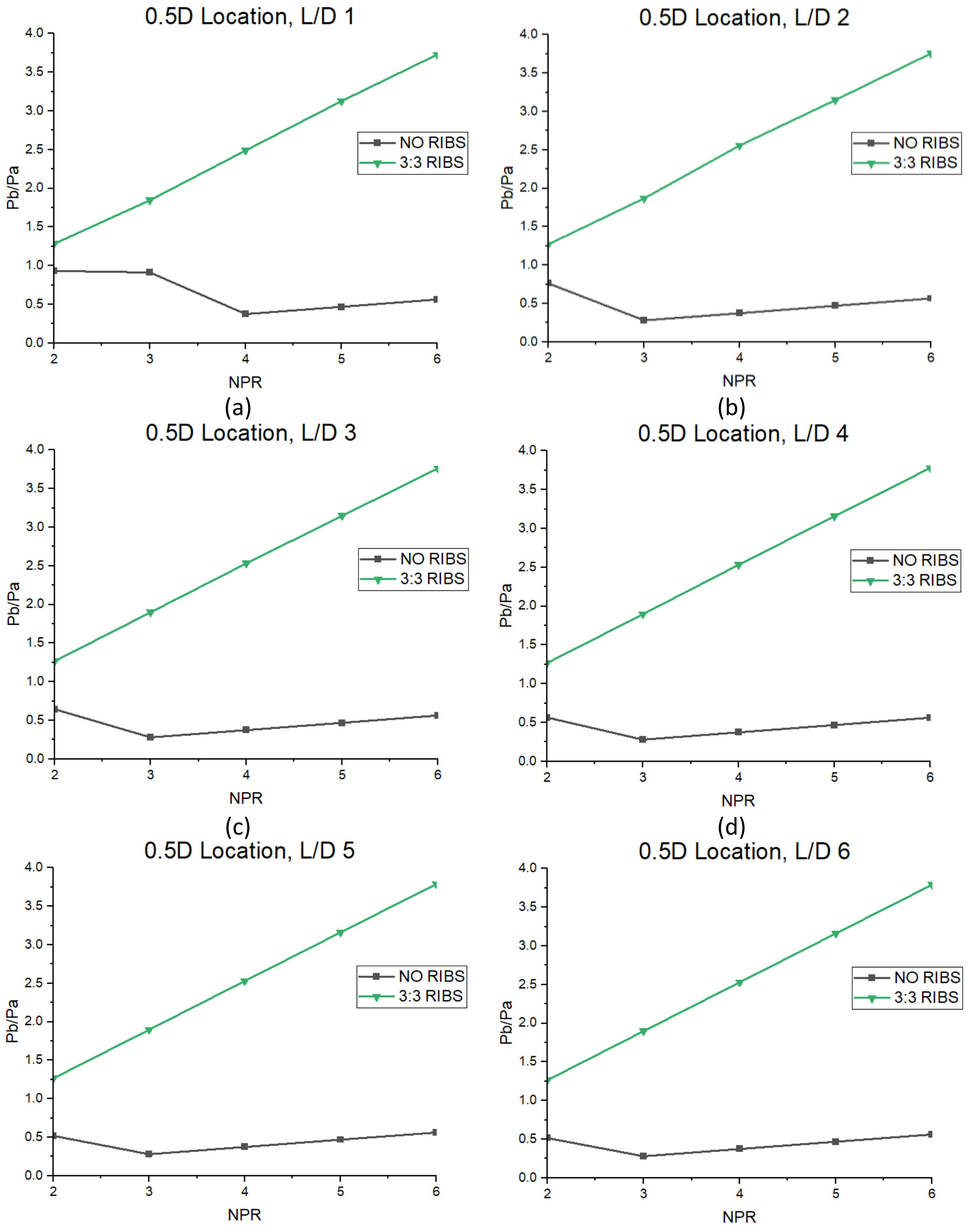

(a) (b) (c) (d) (e) (f)

Fig. 33. The base pressure ratio variations with NPR for rib at 0.5D

Base pressure findings for various duct lengths for a rib location of 1D are shown in Figure 34(a) to Figure 34(e). The results show that without a control case, the base pressure decreases till NPR = 3. Later, for NPR = 3 and above, there is a marginal increase in the base pressure. However, when control is employed, the base pressure has achieved considerable values from NPR 2, which is 25% higher than the atmospheric pressure. The highest NPR = 6 for this study attains a value of 4.5 times the ambient pressure. Similar results are seen for other duct lengths 3D, 4D, 5D, and 6D in Figure 34(b) to Figure 34(e). These results reiterate that the reattachment length for this duct diameter seems to be around 1D. This may be one of the reasons why the base pressure attains a steady state and values do not change even though duct length is varied from L = 2D to 6D.

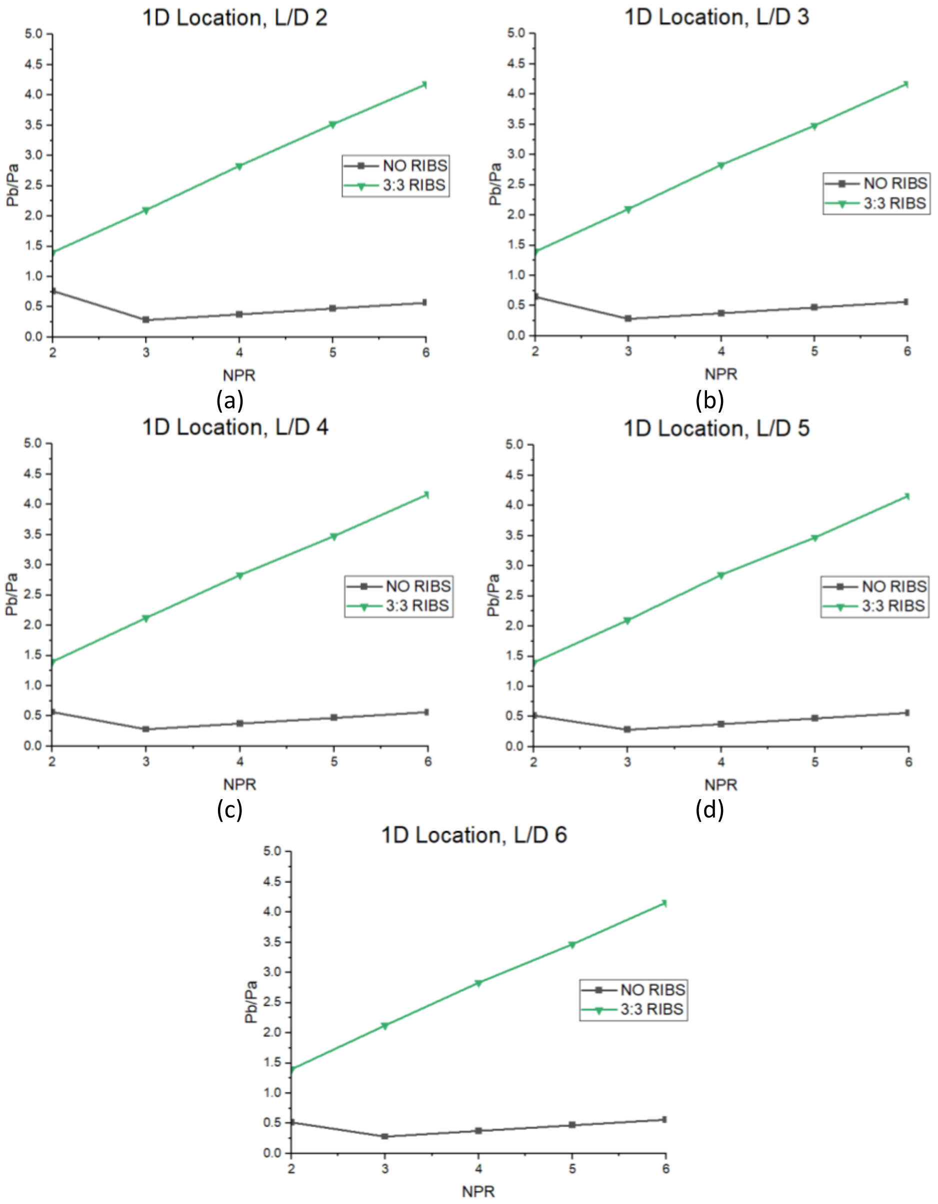

(a) (b) (c) (d) (e)

Fig. 34. The base pressure ratio variations with NPR for rib at 1D

When the ribs are located at 1.5D, the base pressure results are shown in Figure 35(a) to Figure 35(e) for with and without control when the rib's aspect ratio is 3:3. As discussed earlier, since the flow is attached to the enlarged duct wall at around 1D location, any change in the rib placement towards the downstream the rib is moving away from the reattachment point and also from the boundary layer which is growing after getting attached with the duct wall. More so, due to the highest rib height of 3 mm, it may be outside the boundary layer and blocking the main jet exiting from the converging-diverging nozzle. It is also seen that flow behavior without control remains unaltered for all the duct lengths as the flow has attained a steady state at L/d = 2; hence, any change in the duct lengths will not yield any change in the base pressure without control, and same is the situation that with control also, then there is no change in the base pressure values even though there is a change in the duct lengths from 2D to 6D.

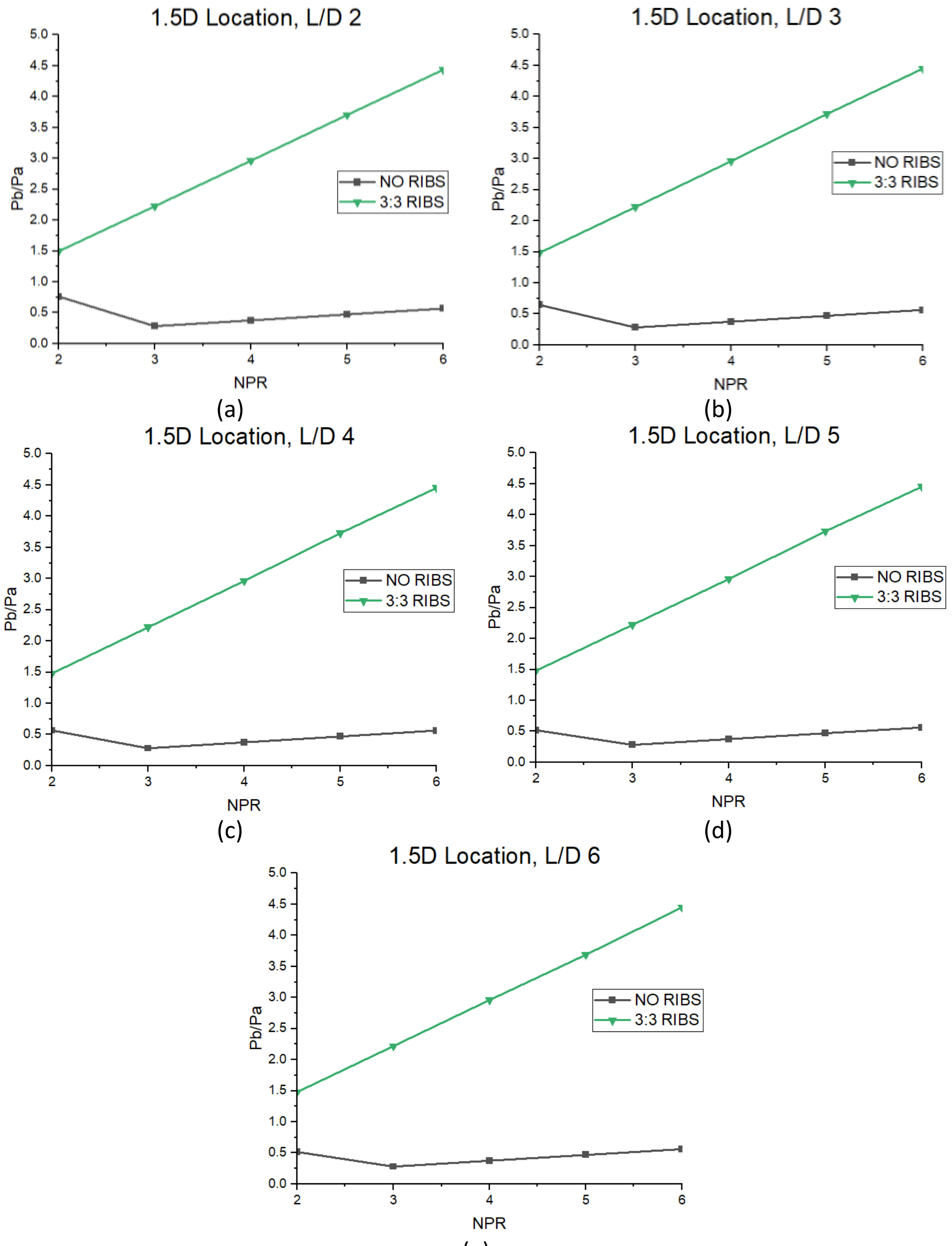

(a) (b) (c) (d) (e)

Fig. 35. The base pressure ratio variations with NPR for rib at 1.5D

When ribs are located at 2D (i.e., 32 mm), the base pressure results without control case are the same for all the duct lengths, as expected (Figure 36). However, when the control in rectangular ribs is placed, there is a 25% increase in the base at NPR = 2. Later, there is a progressive increase in the base pressure, and as high as 4.5 bar is the base pressure value at NPR = 6. Similar results are seen for other duct lengths from 3D to 6D without any change in the base pressure values. The reasons for this trend are the same as discussed earlier.

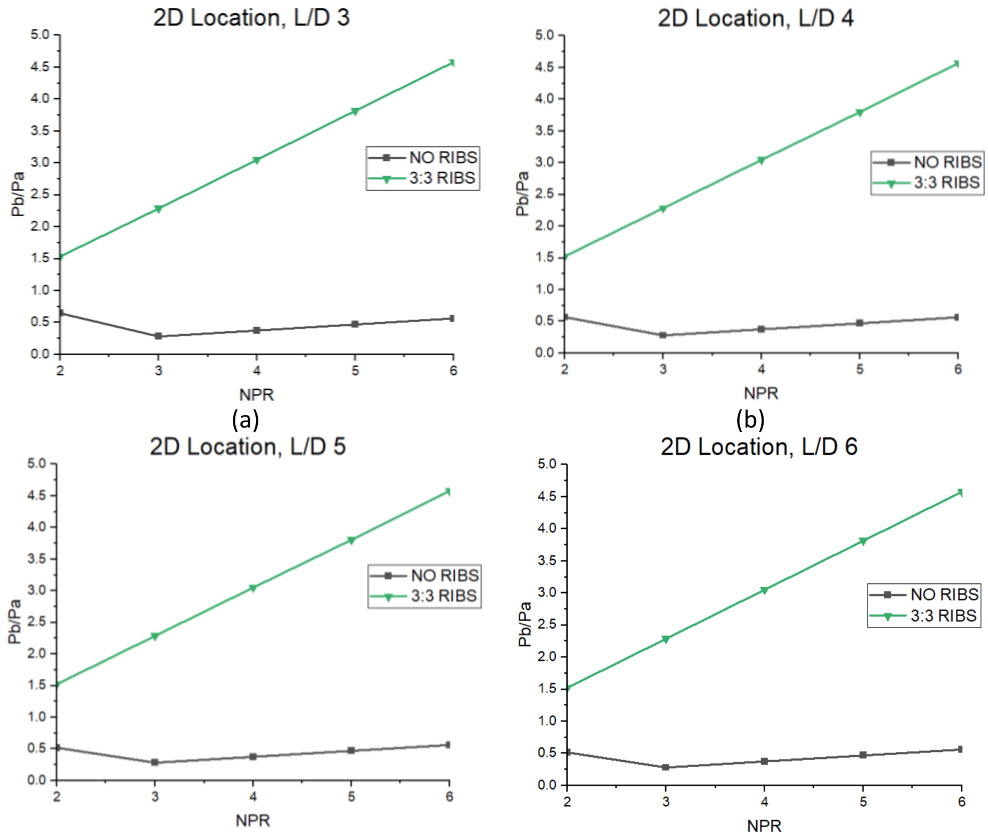

(a) (b)

(c) (d)

Fig. 36. The base pressure ratio variations with NPR for rib at 3D

For Rib placement in 3D, the base pressure results are shown in Figure 37(a) to Figure 37(c) for duct lengths 4D, 5D, and 6D. As discussed earlier, the control placement is further downstream in this case, but this shift downstream cannot impact the base pressure values compared to rib locations 0.5D to 2D. Hence, these results further confirm that the gain while changing the placement of ribs is case-sensitive. Whatever gain we get for rib locations for this duct diameter of 16 mm in the range from 0.5D to 2D, we may not get the same advantage when rectangular ribs are placed at 3D to 4D as we are far away from the reattachment point. Control cannot access the flow field inside the duct, hence the resultant base pressure. Even though this location of the rib has a marginal change in the base pressure, the magnitude of the increase is nominal. Hence, based on the above discussion, we can say that the best rib placement seems to be in the range of 1D to 2D.

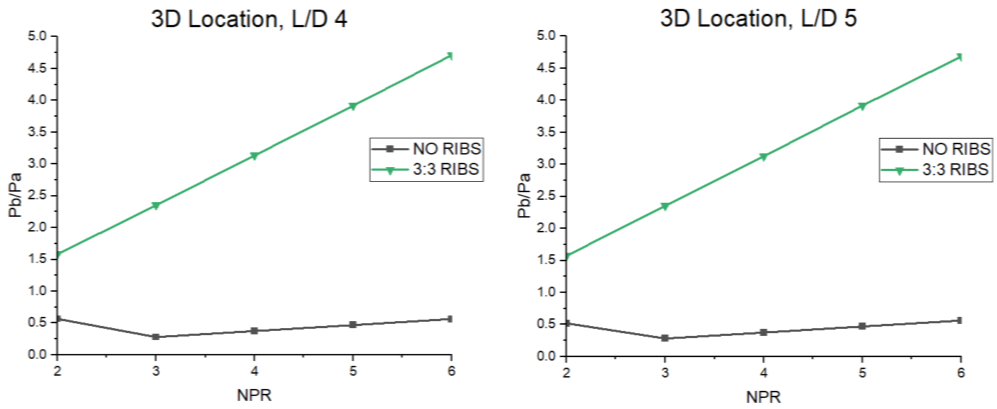

(a) (b)

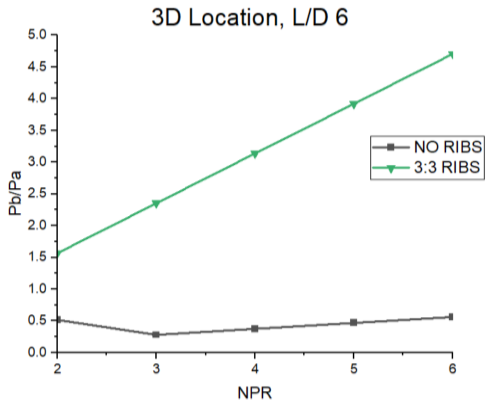

(c)

Fig. 37. The base pressure ratio variations with NPR for rib at 3D

When ribs are placed at 4D for duct lengths 5D and 6D, the results do not show any significant changes. However, there is a marginal increase in the base pressure at NPR = 2 and 6 (Figure 38).

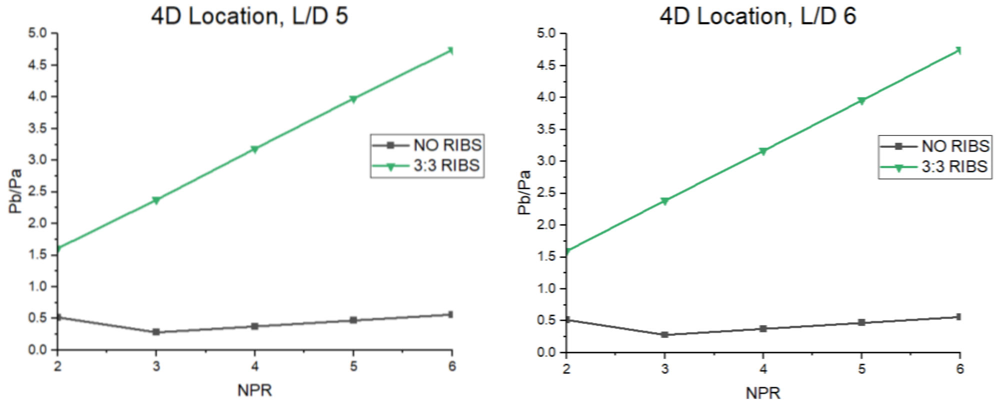

(a) (b)

Fig. 38. The base pressure ratio variations with NPR rib at 4D

4.4 Base Pressure (Pb/Pa) vs Nozzle Pressure Ratio Plot (3:1, 3:2 and 3:3 RIBS)

Figure 39(a) to Figure 39(e) show base pressure results as a function of duct lengths (i.e., L/D) for all three rib sizes (i.e., 3:1, 3:2, and 3:3) for various NPRs in the range from 2 to 6 when ribs are placed at 0.5D. From the results, it is seen that the base pressure attains a steady state at L/D = 3 for NPR = 2, and for remaining NPRs, it attains a steady state at L/D = 1, and this pattern is for rib aspect ratios 3:1 and 3:2, but rib aspect ratio 3:3 the steady state is attained at L/D = 1 itself. This is because rib height is 3 mm and blocks the flow, resulting in a sudden rise in the base pressure.

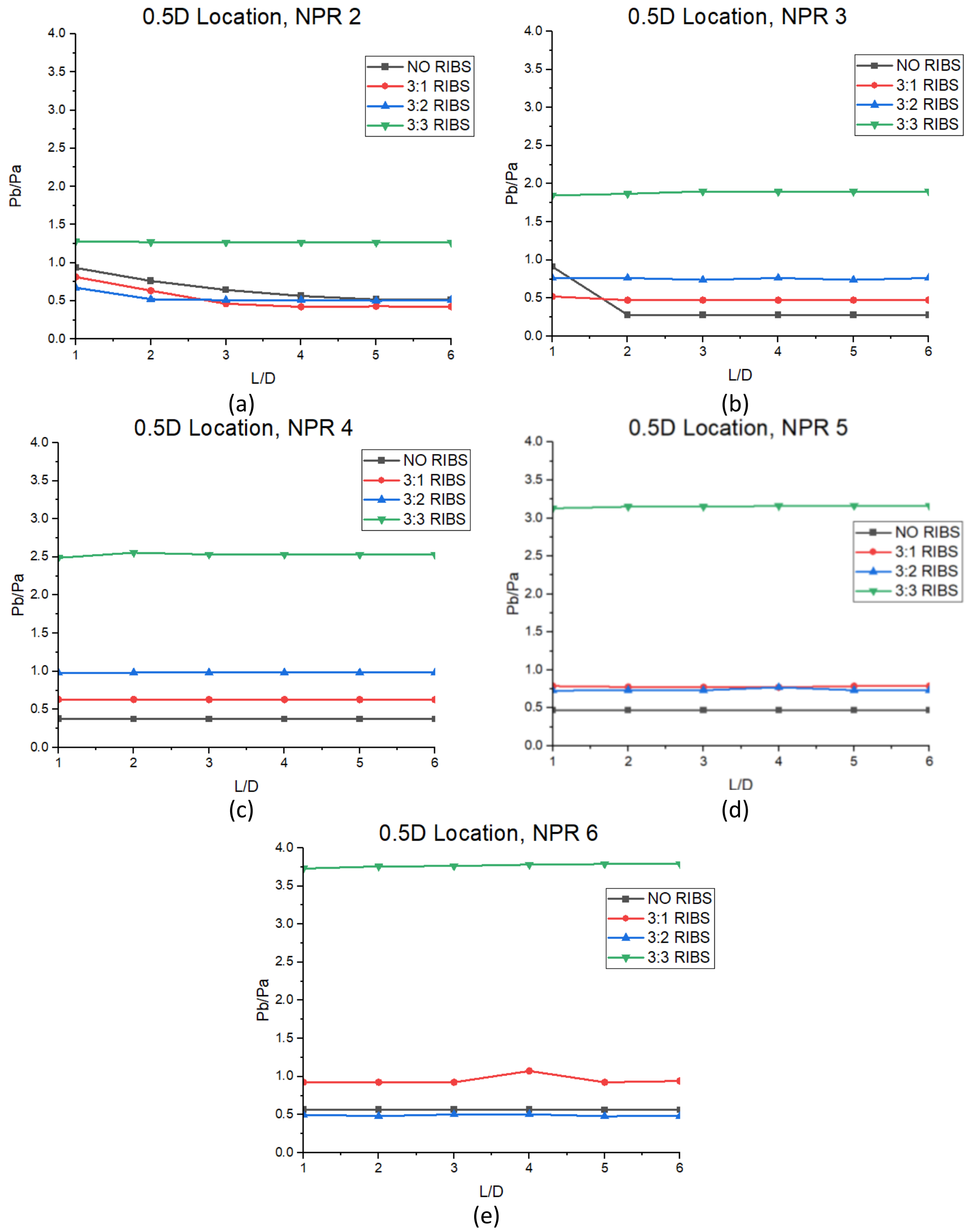

Fig. 39. The base pressure ratio variations with L/D for rib at 0.5D

Figure 40(a) to 40(e) show the base pressure results for rib placement at 1D at various NPRs for all the rib sizes simulated in the study. When NPR = 2, as seen in Figure 41(a), shows an unsteadiness till L/D = 4, later base pressure becomes independent of duct length. At NPR = 2, these results are expected as the nozzle interacts with NPR, which is needed to attain critical conditions. There is also some oscillation in base pressure at NPR = 3, where the level of under-expansion is 1.25. This is bound to happen as the flow passes through the expansion waves. Due to the flow expansion for rib size 3:3, a maximum rise in base pressure is attained at NPR = 6.

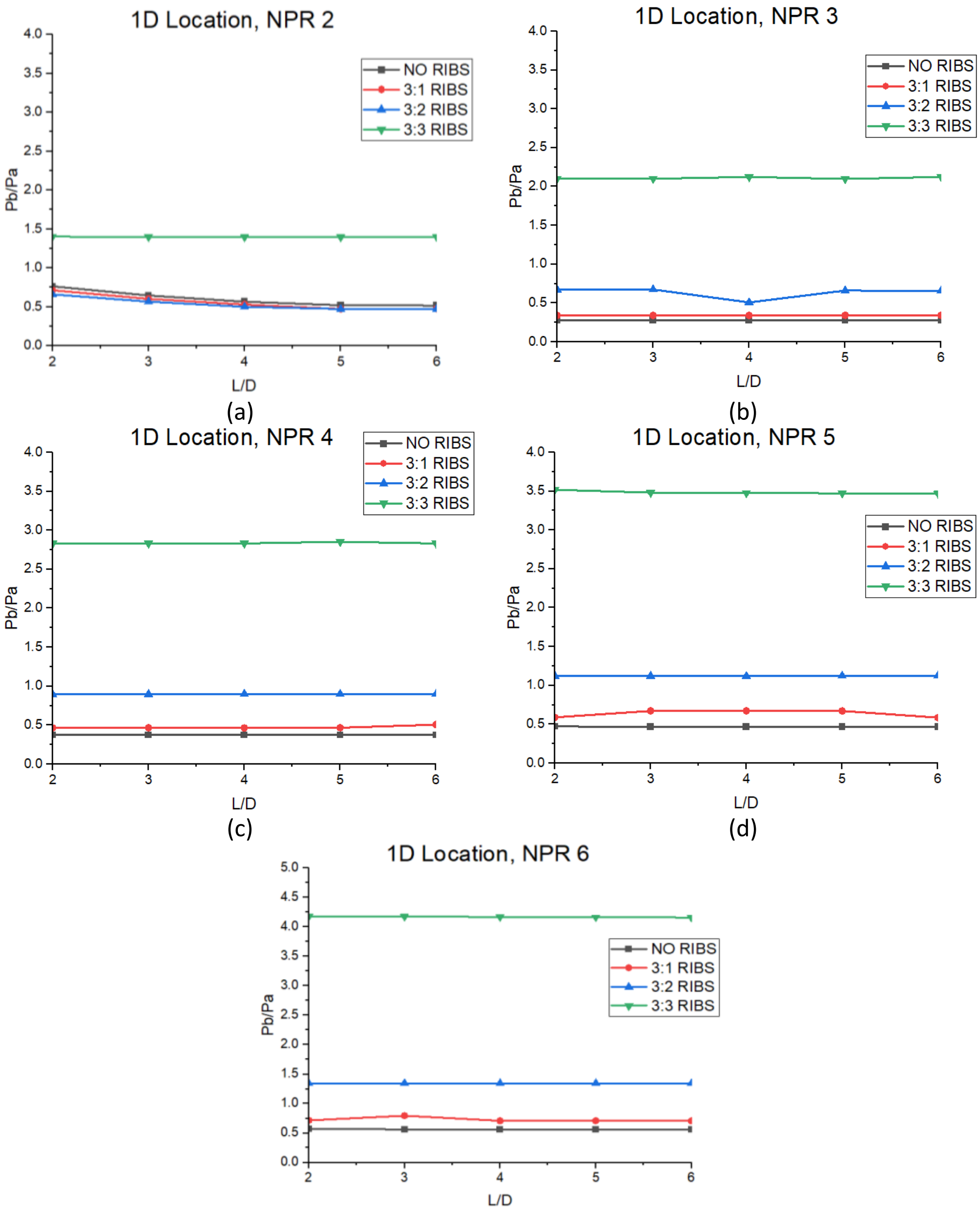

(a) (b) (c) (d) (e)

Fig. 40. The base pressure ratio variations with L/D for rib at 1D

For 1.5D rib locations, the base pressure results are shown in Figure 41(a) to Figure 41(e) for various NPRs. Once again, marginal flow variations are observed at NPR = 2, and the steady state is achieved from L/D = 4. Meanwhile, for NPR greater than 2, the steady state is achieved at L/D = 1, as seen earlier in Figure 41(a). For NPR, more than two, the base pressure becomes independent of duct length right from the beginning, and the base pressure values for ribs are very high, with an aspect ratio of 3:3.

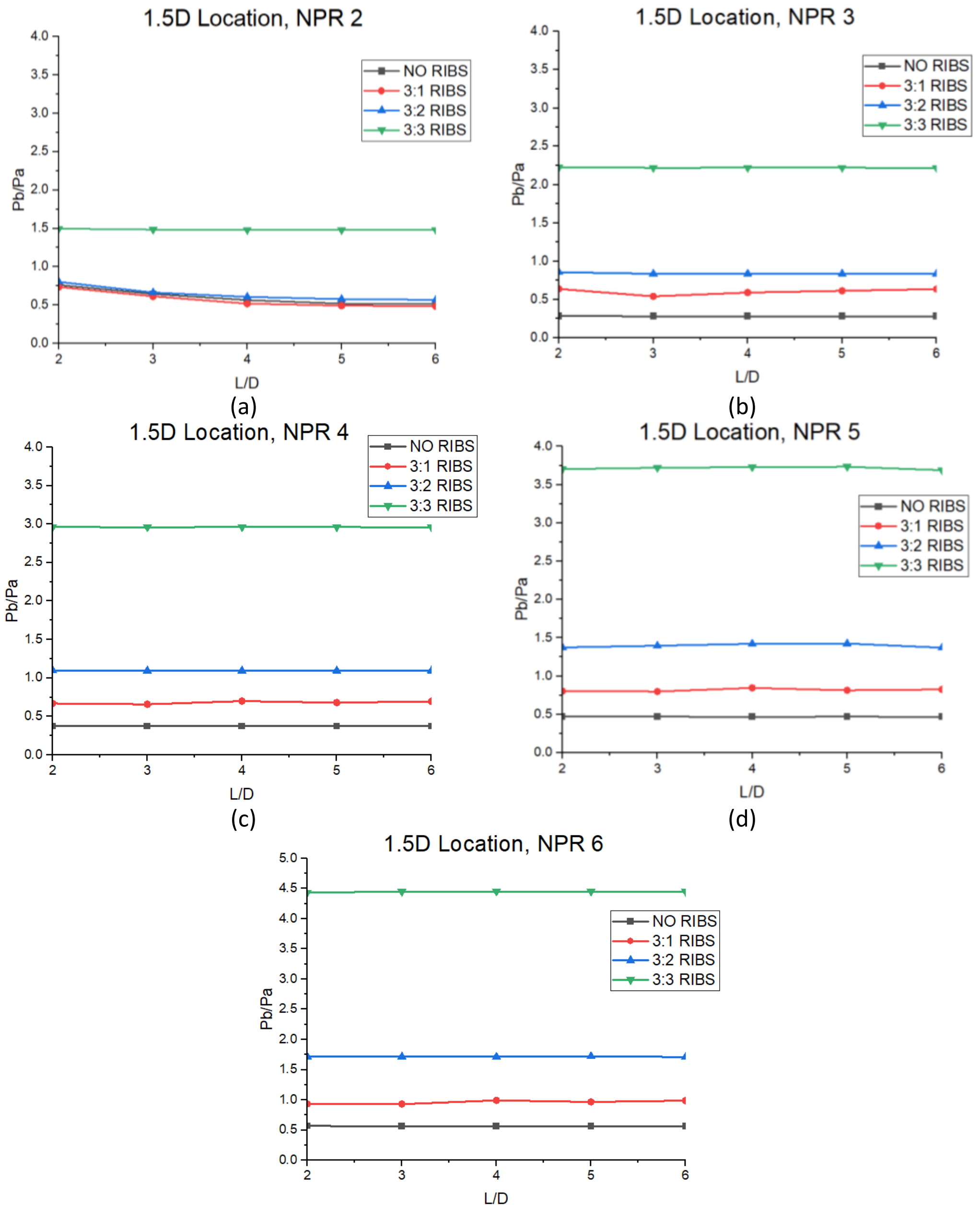

(a) (b) (c) (d) (e)

Fig. 41. The base pressure ratio variations with L/D for rib at 1.5D

Figure 42(a) to 42(e) are shown as a function of duct length at different expansion levels. For this case, the base pressure is independent of duct length right from the beginning, even at NPR = 2. The base pressure results clearly show the impact of the ribs' location in 2D. In the earlier cases where ribs were placed at 0.5D to 1.5D, at NPR 2 and 3, there were some fluctuations in the base pressure values. However, the same phenomenon is not seen for rib locations at 2D. Figure 42(a) shows that base pressure at NPR = 6 1.5 times the ambient pressure. It is also seen that with an increase in the rib's height, there is a considerable increase in the base pressure, but NPR = 6 for ribs with an aspect ratio of 3:3 is the maximum gain, and as high as around 4.5 bar, the base pressure value.

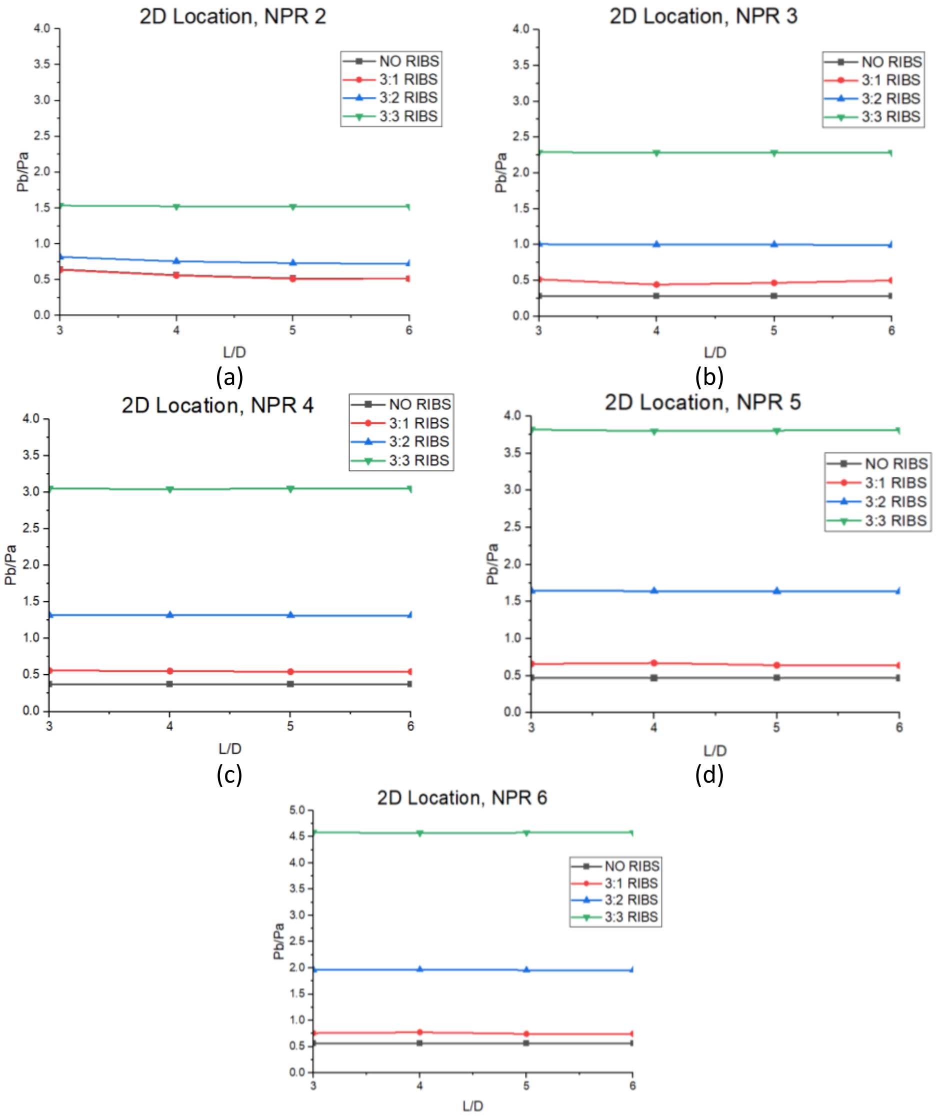

(a) (b) (c) (d) (e)

Fig. 42. The base pressure ratio variations with L/D for rib at 2D

When ribs are placed at 4D locations, the base pressure results as a function of duct length are shown in Figure 43(a) to 43(e) for NPRs ranging from 2 to 6. Figure 43(a) shows results for NPR = 2, indicating that the base pressure results are independent of duct length. However, when we look at the control effectiveness for three ribs having aspect ratios 3:1, 3:2, and 3:3, it is seen that ribs with a 3:1 aspect are marginally effective, the send rib having an aspect ratio 3:2 is more effective, and base pressure for this rib is nearly equal to ambient pressure. However, for ribs with an aspect ratio of 3.3, the base pressure is 1.6 times the ambient pressure. For NPR = 3, there is an increase in the base pressure for aspect ratios 3:2 and 3:3, and their values are 1. 3 times and 2.3 times the ambient pressure, as seen in Figure 43(b).

When we look at the base pressure results at NPR = 4, as shown in Figure 43(c), the base pressure values for these three ribs of height 1 mm, 2 mm, and 3 mm are 07-, 1.7-, and 3.1 times ambient pressure. Similarly, there is a progressive increase in the base pressure values at NPR = 5, as shown in Figure 43(d), and their values for the same values of rib heights are 0.85, 2.1, and 4 times the atmospheric pressure. Likewise, for the highest value of the NPR = 6, as indicated in Figure 43(e), the base pressure values are 1.2, 2.6, and 4.8 times the back pressure.

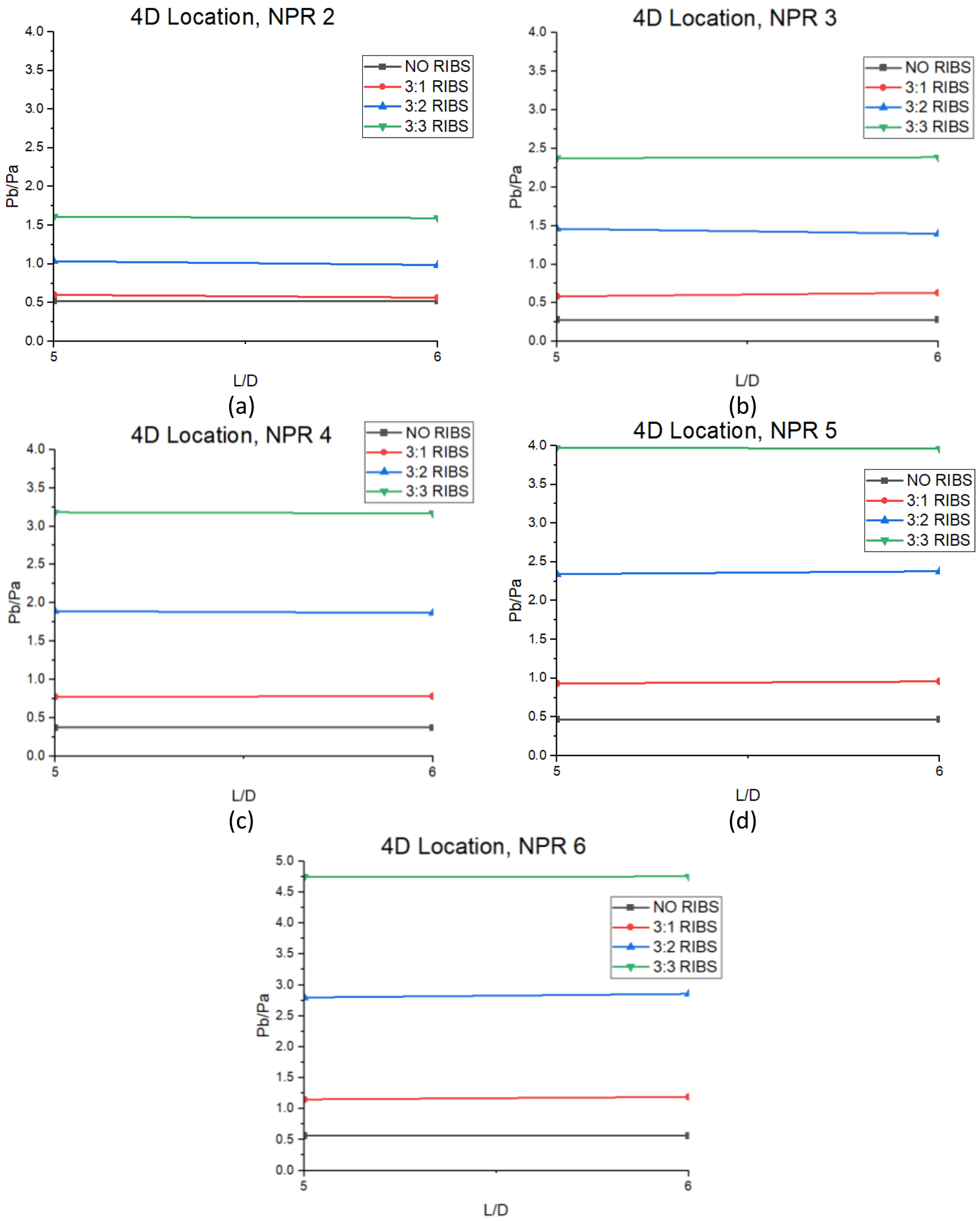

(a) (b) (c) (d) (e)

Fig. 43. The base pressure ratio variations with L/D for rib at 4D

5. Conclusion

The base pressure is influenced by factors such as the level of expansion, Mach number, area ratio, L/D ratio, rib dimensions, and rib location. For suddenly expanded axisymmetric flows, passive controls in the form of annular ribs have significantly reduced the base pressure compared to a plain passage. Annular ribs with aspect ratios of 3:1 and 3:2, compared to 3:3, are efficient in lowering base pressure. At an NPR of 2, the base pressure for ducts with 3:1 and 3:2 ribs is lower than that of the plain duct, indicating that these configurations are most effective at this NPR. As NPR increases, the base pressure also increases. However, at NPR 3 and above, the base pressure for the 3:1 and 3:2 ribs exceeds that of the plain duct, suggesting their effectiveness in reducing base pressure diminishes at higher NPR values. Ribs with an aspect ratio of 3:3 significantly increase base pressure and introduce mild oscillations to the duct pressure field. This behavior is likely due to the geometric characteristics of the 3:3 ribs, which obstruct the flow, leading to increased flow separation and turbulence. This obstruction prevents efficient expansion and mixing of the jet, resulting in elevated base pressure levels. These findings highlight the importance of selecting appropriate rib geometries to optimize aerodynamic performance in ducted systems under different NPR conditions and imply that there is a threshold for the control rib aspect ratio necessary to achieve maximum suction at the base along with minimum pressure loss.

References

[1] Ashfaq, Syed, and S. A. Khan. "The Effect of Micro Jets on Wall Pressure for Sonic under Expanded Flow." *International Journal of Engineering Research and Applications (IJERA)* 4, no. 3 (2014): 32-38.

[2] Vikramaditya, N. S., M. Viji, S. B. Verma, Naveed Ali, and D. N. Thakur. "Base pressure fluctuations on typical missile configuration in the presence of a base cavity." *Journal of Spacecraft and Rockets* 55, no. 2 (2018): 335-345. https://doi.org/10.2514/1.A33926

[3] Schrijer, F. F. J., A. Sciacchitano, and F. Scarano. "Spatio-temporal and modal analysis of unsteady fluctuations in a high-subsonic base flow." *Physics of Fluids* 26, no. 8 (2014). https://doi.org/10.1063/1.4891257

[4] Jukes, Timothy, Takehiko Segawa, and Hirohide Furutani. "Active flow separation control on a NACA 4418 using DBD vortex generators and FBG sensors." In *50th AIAA Aerospace Sciences Meeting including the New Horizons Forum and Aerospace Exposition*, p. 1139. 2012. https://doi.org/10.2514/6.2012-1139

[5] Khan, Sher Afghan, and Ethirajan Rathakrishnan. "Active control of suddenly expanded flows from overexpanded nozzles." *International Journal of Turbo and Jet Engines* 19, no. 1-2 (2002): 119-126. https://doi.org/10.1515/TJJ.2002.19.1-2.119

[6] Khan, Ambareen, Abdul Aabid, and Sher Afghan Khan. "CFD analysis of convergent-divergent nozzle flow and base pressure control using micro-JETS." *International Journal of Engineering and Technology* 7, no. 3.29 (2018): 232-235. https://doi.org/10.14419/ijet.v7i3.29.18802

[7] Fharukh, Ahmed G. M., Abdulrehman A. Alrobaian, Abdul Aabid, and S. A. Khan. "Numerical Analysis of Convergent-Divergent Nozzle using Finite Element Method." *International Journal of Mechanical and Production Engineering Research and Development (IJMPERD)* 8, no. 6 (2018): 373-382. https://doi.org/10.24247/ijmperddec201842

[8] Aabid, Abdul, Ambareen Khan, Nurul Musfirah Mazlan, Mohd Azmi Ismail, Mohammad Nishat Akhtar, and S. A. Khan. "Numerical Simulation of Suddenly Expanded Flow at Mach 2.2." *International Journal of Engineering and Advanced Technology (IJEAT)* 8, no. 3 (2019): 457-462.

[9] Khan, Sher Afghan, Abdul Aabid, and Ahamed Saleel Chandu Veetil. "Influence of micro jets on the flow development in the enlarged duct at supersonic Mach number." *International Journal of Mechanical and Mechatronics Engineering* 19, no. 1 (2019): 70-82.

[10] Pathan, Khizar Ahmed, Prakash S. Dabeer, and Sher Afghan Khan. "Effect of nozzle pressure ratio and control jets location to control base pressure in suddenly expanded flows." *Journal of Applied Fluid Mechanics* 12, no. 4 (2019): 1127-1135. https://doi.org/10.29252/jafm.12.04.29495

[11] Pathan, Khizar Ahmed, Prakash S. Dabeer, and Sher Afghan Khan. "An investigation to control base pressure in suddenly expanded flows." *International Review of Aerospace Engineering (IREASE)* 11, no. 4 (2018): 162-169. https://doi.org/10.15866/irease.v11i4.14675

[12] Pathan, Khizar Ahmed, Sher Afghan Khan, and P. S. Dabeer. "CFD analysis of effect of Mach number, area ratio and nozzle pressure ratio on velocity for suddenly expanded flows." In *2017 2nd International Conference for Convergence in Technology (I2CT)*, pp. 1104-1110. IEEE, 2017. https://doi.org/10.1109/I2CT.2017.8226299

[13] Pathan, Khizar Ahmed, Sher Afghan Khan, and P. S. Dabeer. "CFD analysis of effect of flow and geometry parameters on thrust force created by flow from nozzle." In *2017 2nd International Conference for Convergence in Technology (I2CT)*, pp. 1121-1125. IEEE, 2017. https://doi.org/10.1109/I2CT.2017.8226302

[14] Pathan, Khizar Ahmed, Sher Afghan Khan, and P. S. Dabeer. "CFD analysis of effect of area ratio on suddenly expanded flows." In *2017 2nd International Conference for Convergence in Technology (I2CT)*, pp. 1192-1198. IEEE, 2017. https://doi.org/10.1109/I2CT.2017.8226315

[15] Pathan, Khizar Ahmed, Prakash S. Dabeer, and Sher Afghan Khan. "Investigation of base pressure variations in internal and external suddenly expanded flows using CFD analysis." *CFD Letters* 11, no. 4 (2019): 32-40.

[16] Korst, Helmut Hans. "A theory for base pressures in transonic and supersonic flow." *Journal of Applied Mechanics* 23, no. 4 (1956): 593-600. https://doi.org/10.1115/1.4011405

[17] Anderson, J. S., and T. J. Williams. "Base pressure and noise produced by the abrupt expansion of air in a cylindrical duct." *Journal of Mechanical Engineering Science* 10, no. 3 (1968): 262-268. https://doi.org/10.1243/JMES_JOUR_1968_010_038_02

[18] Khan, Sher Afghan, and E. Rathakrishnan. "Control of suddenly expanded flow." *Aircraft Engineering and Aerospace Technology* 78, no. 4 (2006): 293-309. https://doi.org/10.1108/17488840610675573

[19] Vikramaditya, N. S., M. Viji, S. B. Verma, Naveed Ali, and D. N. Thakur. "Base pressure fluctuations on typical missile configuration in the presence of a base cavity." *Journal of Spacecraft and Rockets* 55, no. 2 (2018): 335-345. https://doi.org/10.2514/1.A33926

[20] Jaimon, D. Q., S. A. Khan, and A. J. Antony. "Effect of flow parameters on base pressure in a suddenly expanded duct at supersonic Mach number regimes using CFD and design of experiments." *Journal of Applied Fluid Mechanics* 11, no. 2 (2018): 483-496.

[21] Khan, S. A., Zakir Ilahi Chaudhary, and Vilas B. Shinde. "Base pressure control by supersonic micro jets in a suddenly expanded nozzle." *International Journal of Mechanical & Mechatronics Engineering* 18, no. 4 (2018): 101-112.

[22] Khan, Sher Afghan, Abdul Aabid, and Maughal Ahmed Ali Baig. "CFD analysis of CD nozzle and effect of nozzle pressure ratio on pressure and velocity for suddenly expanded flows." *International Journal of Mechanical and Production Engineering Research and Development* 8, no. 3 (2018): 1147-1158. https://doi.org/10.24247/ijmperdjun2018119

[23] Khan, Sher Afghan, Abdul Aabid, and C. Ahamed Saleel. "CFD simulation with analytical and theoretical validation of different flow parameters for the wedge at supersonic Mach number." *International Journal of Mechanical and Mechatronics Engineering* 1 (2019).

[24] Pathan, Khizar Ahmed, Prakash S. Dabeer, and Sher Afghan Khan. "Optimization of area ratio and thrust in suddenly expanded flow at supersonic Mach numbers." *Case Studies in Thermal Engineering* 12 (2018): 696-700. https://doi.org/10.1016/j.csite.2018.09.006

[25] Pathan, Khizar Ahmed, Prakash S. Dabeer, and Sher Afghan Khan. "Influence of expansion level on base pressure and reattachment length." *CFD Letters* 11, no. 5 (2019): 22-36.

[26] Chaudhary, Zakir Ilahi, Vilas B. Shinde, and S. A. Khan. "Investigation of base flow for an axisymmetric suddenly expanded nozzle with micro JET." *International Journal of Engineering & Technology* 7, no. 3.29 (2018): 236-242. https://doi.org/10.14419/ijet.v7i3.29.18803

[27] Khan, Sher Afghan, and E. Rathakrishnan. "Control of suddenly expanded flow." *Aircraft Engineering and Aerospace Technology* 78, no. 4 (2006): 293-309. https://doi.org/10.1108/17488840610675573

[28] Shaikh, Sohel Khalil, Khizar Ahmed Pathan, Zakir Ilahi Chaudhary, B. G. Marlpalle, and Sher Afghan Khan. "An investigation of three-way catalytic converter for various inlet cone angles using CFD." *CFD Letters* 12, no. 9 (2020): 76-90. https://doi.org/10.37934/cfdl.12.9.7690

[29] Shaikh, Sohel Khalil, Khizar Ahmed Pathan, Zakir Ilahi Chaudhary, and Sher Afghan Khan. "CFD analysis of an automobile catalytic converter to obtain flow uniformity and to minimize pressure drop across the monolith." *CFD Letters* 12, no. 9 (2020): 116-128. https://doi.org/10.37934/cfdl.12.9.116128

[30] Pathan, Khizar A., Prakash S. Dabeer, and Sher A. Khan. "Enlarge duct length optimization for suddenly expanded flows." *Advances in Aircraft and Spacecraft Science* 7, no. 3 (2020): 203-214. https://doi.org/10.12989/aas.2020.7.3.203

[31] Pathan, Khizar Ahmed, Syed Ashfaq, Prakash S. Dabeer, and Sher Afgan Khan. "Analysis of Parameters Affecting Thrust and Base Pressure in Suddenly Expanded Flow from Nozzle." *Journal of Advanced Research in Fluid Mechanics and Thermal Sciences* 64, no. 1 (2019): 1-18.

[32] Pathan, Khizar, Prakash Dabeer, and Sher Khan. "An investigation of effect of control jets location and blowing pressure ratio to control base pressure in suddenly expanded flows." *Journal of Thermal Engineering* 6, no. 2 (2019): 15-23. https://doi.org/10.18186/thermal.726106

[33] Khalil, Shaikh Sohel Mohd, Rai Sujit Nath Sahai, Nitin Parashram Gulhane, Khizar Ahmed Pathan, Ajaj Rashid Attar, and Sher Afghan Khan. "Experimental Investigation of Local Nusselt Profile Dissemination to Augment Heat Transfer under Air Jet Infringements for Industrial Applications." *Journal of Advanced Research in Fluid Mechanics and Thermal Sciences* 112, no. 2 (2023): 161-173. https://doi.org/10.37934/arfmts.112.2.161173

[34] Jain, Yogeshkumar, Vijay Kurkute, Sagar Mane Deshmukh, Khizar Ahmed Pathan, Ajaj Rashid Attar, and Sher Afghan Khan. "The Influence of Plate Fin Heat Sink Orientation under Natural Convection on Thermal Performance: An Experimental and Numerical Study." *Journal of Advanced Research in Fluid Mechanics and Thermal Sciences* 114, no. 2 (2024): 118-129. https://doi.org/10.37934/arfmts.114.2.118129

[35] Pathan, Khizar Ahmed, Zakir Ilahi Chaudhary, Ajaj Rashid Attar, Sher Afghan Khan, and Ambareen Khan. "Optimization of Nozzle Design for Weight Reduction using Variable Wall Thickness." *Journal of Advanced Research in Fluid Mechanics and Thermal Sciences* 112, no. 2 (2023): 86-101. https://doi.org/10.37934/arfmts.112.2.86101

[36] Pathan, Khizar A., Sher A. Khan, N. A. Shaikh, Arsalan A. Pathan, and Shahnawaz A. Khan. "An investigation of boattail helmet to reduce drag." *Advances in Aircraft and Spacecraft Science* 8, no. 3 (2021): 239-250. https://doi.org/10.12989/aas.2021.8.3.239

[37] Khan, Sher Afghan, M. A. Fatepurwala, K. N. Pathan, P. S. Dabeer, and Maughal Ahmed Ali Baig. "CFD analysis of human powered submarine to minimize drag." *International Journal of Mechanical and Production Engineering Research and Development (IJMPERD)* 8, no. 3 (2018): 1057-1066. https://doi.org/10.24247/ijmperdjun2018111

[38] Aqilah, Nur, Khizar Ahmed Pathan, and Sher Afghan Khan. "Passive Control of Base Flow at Supersonic Mach Number for Area Ratio 4." In *International Conference on Advances in Heat Transfer and Fluid Dynamics*, pp. 37-50. Singapore: Springer Nature Singapore, 2022. https://doi.org/10.1007/978-981-99-7213-5_4

[39] Fiqri, Muhammad Ikhwan, Khizar Ahmed Pathan, and Sher Afghan Khan. "Control of Suddenly Expanded Flow with Cavity at Sonic Mach Number." In *International Conference on Advances in Heat Transfer and Fluid Dynamics*, pp. 3-15. Singapore: Springer Nature Singapore, 2022. https://doi.org/10.1007/978-981-99-7213-5_1

[40] Khan, Sher Afghan, Abdul Aabid, Imran Mokashi, Abdulrahman Abdullah Al-Robaian, and Ali Sulaiman Alsagri. "Optimization of two-dimensional wedge flow field at supersonic Mach number." *CFD Letters* 11, no. 5 (2019): 80-97.

[41] Shamitha, Shamitha, Asha Crasta, Khizar Ahmed Pathan, and Sher Afghan Khan. "Analytical and Numerical Simulation of Surface Pressure of an Oscillating Wedge at Hypersonic Mach Numbers and Application of Taguchi's Method." *Journal of Advanced Research in Applied Sciences and Engineering Technology* 30, no. 1 (2023): 15-30. https://doi.org/10.37934/araset.30.1.1530

[42] Shamitha, Shamitha, Asha Crasta, Khizer Ahmed Pathan, and Sher Afghan Khan. "Numerical simulation of surface pressure of a wedge at supersonic Mach numbers and application of design of experiments." *Journal of Advanced Research in Applied Mechanics* 101, no. 1 (2023): 1-18. https://doi.org/10.37934/aram.101.1.118

[43] Shaikh, Javed S., Krishna Kumar, Khizar A. Pathan, and Sher A. Khan. "Computational analysis of surface pressure distribution over a 2d wedge in the supersonic and hypersonic flow regimes." *Fluid Dynamics & Materials Processing* 19, no. 6 (2023). https://doi.org/10.32604/fdmp.2023.025113

[44] Shaikh, Javed Shoukat, Khizar Ahmed Pathan, Krishna Kumar, and Sher Afghan Khan. "Effectiveness of Cone Angle on Surface Pressure Distribution along Slant Length of a Cone at Hypersonic Mach Numbers." *Journal of Advanced Research in Fluid Mechanics and Thermal Sciences* 104, no. 1 (2023): 185-203. https://doi.org/10.37934/arfmts.104.1.185203

[45] Shaikh, Javed S., Krishna Kumar, Khizar A. Pathan, and Sher A. Khan. "Analytical and computational analysis of pressure at the nose of a 2D wedge in high speed flow." *Advances in Aircraft and Spacecraft Science* 9, no. 2 (2022): 119-130. https://doi.org/10.12989/aas.2022.9.2.119

[46] Rathakrishnan, E. "Effect of ribs on suddenly expanded flows." *AIAA Journal* 39, no. 7 (2001): 1402-1404. https://doi.org/10.2514/2.1461